Fatigue and Fracture of Nanocrystalline Metals (Experiments and Simulation)

A Dissertation Report

Submitted in the partial fulfilment of the requirement for the award of the degree of

Master of Technology

In

Nanotechnology

By

Preet Kumar

(14551009)

Centre of Nanotechnology

Indian Institute of Technology

Roorkee (India) – 247667

May, 2016

Abstract

Magnesium alloys are attracting engineers for their practical applications to the industrial use because of its light weight and high specific strength. In this work, fatigue- fracture properties, as they are the most important mechanical property of any material for its structural use, have been examined for Magnesium ZE41 alloy processed under different conditions. Magnesium ZE41 alloy is mainly used in the aviation industry, so fatigue and fracture properties are very crucial for the material to be used for these applications. Tensile strength and Vickers Hardness of the alloys was examined for different processed samples. Fracture toughness of the processed and unprocessed alloy was find out by conducting 3-point bend test. The experimental results were verified by performing finite element simulations, using ANSYS software. The simulation results were found quite similar to the experimental results. Fracture mechanics simulations were carried out for edge cracked, center cracked and double edge cracked specimen to find out the effect of processing on the alloy. There was a clear increment in the fracture strength of the alloy after high strain rolling at high temperature. The strength of the alloy showed maximum increment of more than 200% for 3-pass forging followed by 70% rolling condition. The ductility of the alloy showed maximum increment of about 400% for 6-pass forging followed by 70% rolling condition. Microstructural examination of the processed alloy showed the alloy possessed an ultrafine grained structure after 3-pass forging followed by 70% rolling with grain size of approximately 800nm and also after 6-pass of forging with grain size of approximately 700nm. TEM observations were carried out for the submicron level feature of the processed alloy. Fractrography of the broken tensile samples were carried out using SEM, showed that the mechanism of fracture after application of high strain deformation was mainly grain boundary sliding. Fatigue simulations were carried out using ANSYS software for different condition processed alloys. There was a clear improvement in the fatigue life of the alloy because of the increase in both strength and ductility of the alloy.

Candidate's Declaration

I hereby declare that the proposed work presented in this dissertation entitled **"Fatigue and Fracture of Nanocrystalline Metals (Experiment and Simulation)"** is in the partial fulfilment of the requirements for the award of the degree of Master of Technology in Nanotechnology, submitted in the Centre of Nanotechnology, Indian Institute of Technology Roorkee is an authentic record of my own work carried out during the period from July 2015 to May 2016 under the supervision of **Dr. R Jayaganthan,** Professor, MMED & Centre of Nanotechnology and **Dr. M. M. Mahapatra,** Associate Professor, Mechanical and Industrial Engineering Department, Indian Institute of Technology Roorkee, India.

The data presented in this dissertation has not been submitted by me for the award of any other degree.

Dated:

Place: IIT Roorkee **(Preet Kumar)**

Certificate

This is to certify that the above statement made by the candidate is correct to the best of my knowledge and belief.

Dr. R. Jayaganthan

Professor

MMED & Centre of Nanotechnology

IIT Roorkee, India-247667

Dr. M. M. Mahapatra

Associate Professor

MIED

IIT Roorkee, India- 247667

Acknowledgment

First of all I would like to thank my parents for their blessings and support that gave me enough courage to complete this dissertation work successfully. I take this opportunity to express with the utmost gratitude and sincere thanks to **Dr. R. Jayaganthan,** Professor, Metallurgical and Materials Engineering Department & Centre of Nanotechnology, IIT Roorkee and **Dr. M. M. Mahapatra,** Associate Professor, Mechanical and Industrial Engineering Department, IIT Roorkee for their expert and kind guidance to my dissertation work. My work would have been directionless without their constant and patient guidance. Their invaluable guidance and support throughout this work cannot be put down in few words and will always as a moral support for me in future.

It is my pleasure to express my sincere gratitude to former Head of Department, Metallurgical and Materials Engineering Department and Head, Centre of Nanotechnology, IIT Roorkee, **Dr. S. K. Nath** for providing all the facilities required to carry out this work in the department.

I would like to thank **Mr. Sankulp Goel, Mr. Nikhil Kumar, Ms. Devashri Flouria, Mr. Yogesha K. K., Mr. Amit Joshi, Mr. Raviraj Verma** and **Mr. Vikas Aggarwal** for their co-operation and encouragement at every stage of this work.

I would like to thank all the **Technical Staff** at the Centre of Nanotechnology, IIT Roorkee and Department of Metallurgical and Materials Engineering (MMED), IIT Roorkee, for helping me to access the labs and equipment. Last but not the least I would like to thank my family and friends for their constant moral support during the project work.

Date:

Place: IIT Roorkee **(Preet Kumar)**

Table of Contents

List of Tables

List of Figures

Chapter 1: Introduction

1.1 Motivation

Magnesium Alloys are getting a lot of attention now a days because of its excellent properties like lowest density among all structural materials, highest specific strength, suitability for die casting, high speed machining and also easy availability [1]. But the use of these alloys are limited because of its low ductility at room temperature, low elastic modulus, limited cold working and toughness, limited strength and creep resistance at higher temperatures, high shrinkage during solidification in casting, high chemical reactivity and limited corrosion resistance [1]. The limited ductility of magnesium is due to its lesser numbers of slip systems available at room temperature. For this reason only high temperature processing methods can be applied to it.

Magnesium alloys found their applications in many fields other than structural applications such as biomedical implants [3], battery cells and other electronic applications [20], [21]. The most important use of magnesium alloys is in aviation industry where the weight loss is very crucial. Use of magnesium alloys in automobiles and other structural applications can save a lot of energy due to loss in weight.

Many magnesium alloys have been developed so far and scientists are working on new alloys for better mechanical properties. The magnesium alloy ZE41 came into existence in the 1940s [19]. It is the casting alloy of magnesium containing rare earths. This alloy has a very good combination of properties, it is used in the aviation industry to reduce the weight of the aircraft. The main concern of this alloy was its low corrosion resistance. So, mostly the studies on this alloy were focussed on the corrosion improvement of this alloy using different surface treatment processes. There is a lot of literature available on the surface treatment of this alloy and also on the biocompatibility in the human body [3]. But most of the applications of this alloy are in as casted form. A few work has been done to improve its mechanical and physical properties by using some processing techniques [11], [12], [13]. The method used for the processing on this alloy is ECAP. The problem of ECAP is that it requires a large number of passes, nearly 60 [13], to get a uniform homogeneous microstructure.

Recently many ultrafine grained/Nano-grained materials such as aluminium alloys, titanium alloys, pure titanium, zirconium etc. are produced through SPD processing such as ECAP (Equal

Channel Angular Pressing), HPT (High Pressure Torsion), MAF (Multi Axial Forging), ARB (Accumulative Roll Bonding) [25], Cryo-rolling (CR) [26], etc. have been reported. These materials have better properties than conventional materials. Among these processes mostly studies available for magnesium alloys is ECAP because of it is easy to use and can be easily industrialised [11], [12], [13]. Some studies are also there for Multi-Axial forging (MAF) [10], [14], ARB [22] and HPT [23].

The problem with magnesium and its alloys is that it has only two slip systems available at room temperature, so cold working is not possible for this material. Only high temperature processing can be applied to magnesium and its alloys. The grain refinement mechanism at higher temperature is only dynamic recrystallization [7], [8], [9]. The SPD processing requires the application of a very large strain, hence high temperatures above than recrystallization temperature is required for SPD processing of magnesium and its alloys.

MAF can be used as the SPD technique to produce ufg magnesium ZE41 alloy. The advantage with using MAF is that this process can be easily industrialized to produce bulk materials and it requires very less number of passes to get homogeneous uniform microstructure [13], [10]. A few research has been done on ZE41 alloy processed thorough SPD, which is only ECAP. So, there is advantage using MAF as the SPD technique for producing ultrafine grained ZE41 alloy. For structural applications the tensile strength, hardness and fracture toughness are very important properties.

Finite Element Analysis (FEA) is getting a lot of attention now a days because of its wide range of applications in the analysis of different structures or bodies through simulation using Finite Element Method (FEM). The simulations are carried out using the boundary conditions which replicate the original working condition of the object. It saves a lot of resources because actual model testing of a prototype will require a lot of material and manpower consumption and testing will also take a lot of time. The FEA was first used in the aviation industry, then it was widely used in World War II for testing jets, missiles and space flights. Now it has been evolved to every field of industry.

To solve the fracture mechanics problems a lot of numerical methods have been proposed in last many years. Among these methods FEM is the most popular method for carrying out fracture mechanics simulations. It is a very powerful and mature method [26], and it can deal with very

complex geometry, contact conditions and material behaviours. Another type of method used for fracture mechanics analysis is the boundary element method (BEM). In this method the governing partial derivative equations are solved once when they are formulated in terms of integral equations [27], [28]. Among other methods for fracture mechanics, the generalized finite element method [30] and the extended finite element method (XFEM) [31] are worth to be mentioned. Particularly for fracture mechanics applications, the methods based on the partition of unity [29] are also very much used.

Hence the present objective of this dissertation work is to produce ultrafine grained ZE41 magnesium alloy using MAF at high temperatures and find out the mechanical behaviour of this processed alloys through tensile testing, Vickers hardness and fracture behaviour testing. The deformation behaviour was analysed using optical and TEM microstructural studies and the fracture behaviour was understood through fractrography using SEM. Finite Element Simulations were carried out using Finite element software ANSYS 15.0. Simulations were performed for verifying the results obtained from the experimental testing. Fatigue and fracture simulations were carried out to see the behaviour of the material after different processing routes.

Chapter 2: Literature Review

2.1 Introduction

This chapter is provided to get a knowledge of magnesium alloys and its strengthening mechanisms and also give idea about development of ultrafine grained materials using SPD techniques like Equal Channel Angular Pressing (ECAP), Accumulative Roll Bonding (ARB), Multiaxial Forging (MAF), High Pressure Torsion (HPT), etc.

2.2 Magnesium

Magnesium is the lightest structural material, having density of 1.74g/$cm^{3.}$ It is mostly used as an alloying element in many materials including casting, forging, extrusion, rolled sheets and plates. Earth's crust consists of nearly 2.7% of magnesium. Magnesium is found in the form of dolomite ($MgCO_3.CaCO_3$), carbonate, magnesite ($MgCO_3$) and also in the form of carnallite ($MgCl_2.KCl.6H_2O$) in the salt lakes, but it is not found in metallic form. However its major source is sea water (0.13% of world's sea) [2].

Sir Humphery Davy, in 1808 recognised that magnesium oxide was oxide of new metal magnesium. Magnesium metal was first isolated by a French scientist Alexander Bussy in 1828. He fused magnesium chloride with metallic potassium to get metallic magnesium. The first production of magnesium was done using electrolytic reduction of chloride by Michael Faraday in 1833 [2]. Two basic processes are used now a days to produce magnesium metal: 1) electrolytic reduction of fused anhydrous $MgCl_2$, 2) thermal reduction of magnesium oxide (MgO) using ferrosilicon derived from carbonate ores.

2.3 Alloys of Magnesium

Magnesium is most commonly used as alloying element with other metals for structural applications. Most common alloying elements are: Aluminium, Beryllium, Calcium, Cerium, Copper, Manganese, Nickel, Neodymium, Rare Earth Metals, Silicon, Strontium, Tin, Yttrium, Zinc and Zirconium. Zirconium is mainly used as grain refiner. [2]

2.4 Applications

There are a wide range of applications of magnesium and its alloys which are as follows [2]:

- Magnesium powder has been used flares for night aerial photography, fireworks, high energy fuels and incendiary devices.

- Cathodic protection, batteries both dry cell and reverse cell type such as sea water activated cell, and photoengraving.
- Elevated temperature properties in missiles and aircrafts
- Fatigue strength in wheels
- Damping in electronic housing for aircraft and missiles
- Dimensional stability in electronic housing and in jigs and fixtures
- Machinability in tooling plate
- Dent resistance in luggage
- Non marking qualities in textile machinery
- Low resistance to passage to X-rays and thermal neutrons in x-ray cassettes
- Nuclear fuel cans.
- Orthopaedic implants
- Military products mainly missiles, frames of shelter and bases used for mortar,
- Frames, floors, wheels, panels, brackets and engine components such as piston and housings for aircraft and surface vehicles.

2.5 Designation of Magnesium alloys

The most widely used designation system is that of the American Society for Testing and Materials (ASTM). The method is a four part letter-number system expressed as follows [2]:

(i) the two first letters specify the principal alloying elements in order of reduced content, where: A– Aluminium, B– Bismuth, C– Copper, D– cadmium, E– rare earth, H– thorium, K– Zirconium, L– Lithium, M– Manganese, N– Nickel, P– Lead, Q– Silver, S– silicon, T– Tin, Y– Yttrium and Z– Zinc;

(ii) two numbers shows the round-off percentages of two principal alloying elements;

(iii) a letter for the distinction between alloys having same base chemistry;

(iv) The letter following number, that indicates the temper condition where:

- F for fabricated alloys,
- O: Annealed or wrought alloys,
- H: Strain hardened alloys,
- T–thermally treated other than F, O and H; following number indicates the specific temper.

2.6 Magnesium ZE41 Alloy

ZE41 is the casting alloy of magnesium which contains zinc, zirconium and rare earths. The alloy is high integrity casting alloy that can operated room temperature or up to 150°C. It came into existence in late 1940s. It is also known as the aeronautic magnesium alloy because it is mostly used in the aviation industry. The chemical composition of the alloy is as shown in Table 2.1.

Table 2.1 Chemical composition of ZE41 Mg alloy [38].

Alloying Element	Standard Composition (weight %)
Zinc	3.5 - 5.0
Zirconium	0.4-1.0
Total rare earth	0.8 – 1.70
Manganese	0.15 Max
Iron	0.01 Max
Copper	0.03 Max
Nickel	0.005 Max
Silicon	0.01 Max
Magnesium	Remainder

The Mg ZE41 alloys is extensively used in the aviation industry from a very long time [19]. The alloy is mainly used in the casting form. The industrial applications includes transmission of Sikorsky UH60 Family (Blackhawk) Helicopter with ½ hour dry run capacity, Boeing H47 Chinook Helicopter, Boeing AH64 Apache Helicopter, Bombardier Q Series Dash 8, PW150 Series- 7000 SHP class, Pratt & Whitney Canada PWC 100 Series Turboprop, EMB ERJ, Global Hawk, Citation X, Rolls-Royce Allison AE- 3007, Cessna Citation Excel, PW535 Turbofan Pratt & Whitney Canada, Hamilton Sundstrand F16 AMAD, EFV Transmission Castings and many more [19].

Aibin et al. [13] reported increase in both strength and ductility in UFG ZE41 alloy produced using ECAP process at 330°C. Multi pass ECAP produced the grain refinement in the HCP- structured Mg ZE41 alloy at elevated temperature undergoing by dynamic recrystallization, which increases both strength and the ductility at room temperature because of higher fraction of the high angle grain boundaries and lower intergranular dislocation density. Rengen et al. [12] observed

refinement in both grain and particle size of ZE41 alloy produced through ECAP. Both Strength and ductility increment was observed and two type of twinning {1 0 1^{-} 2} and {1 0 1^{-} 1} were also observed due to ECAP.

Table 2.2 Physical properties of Mg ZE41 Alloy [38].

Property	**Value**
Specific Density	1.84 g/cm^3
Melting Point	510°C-640°C
Tensile Strength	200 MPa
Modulus of Elasticity	44.1 GPa
Poisson's Ratio	0.35
Elongation to Failure	3%
Brinell Hardness	55-70
Coefficient of thermal Expansion	27.1 × 10^{-6}K^{-1}
Corrosion rate	4–6 mg/cm^2/day 320–480 mpy
Thermal conductivity	109W/mK
K_{IC}	15.1-16.3 MPa/m$^{1/2}$

2.7 Severe Plastic Deformation

Severe plastic deformation (SPD) processes may be defined as the metal forming processes in which very large amount of plastic strain is applied on the bulk material. The main aim of SPD processing is production of ultrafine grained material [39]. Many SPD techniques have been developed so far for the production of ultrafine grained materials with superior mechanical and physical properties. Some of these processes includes ECAP, ARB, HPT, MAF etc. [39].

Segal proposed ECAP in 1977 in order to produce ultrafine grained materials. Azushima et al. proposed the repetitive side extrusion process in which high back pressure is applied. Nishida et al. developed a rotary die ECAP process, in which the die contains two channels with the same cross section intersecting at the centre of the die at right angles to remove the limitations of conventional ECAP of removing material after each pass. Rosocchowski et al. proposed

Incremental ECAP process, in which incremental feeding is done in a reciprocating die whose movement is synchronised with feeding [39].

Saito et al. proposed the ARB process, in which the stacking of sheets and conventional roll bonding is performed. A strip is neatly placed on the top of another strip for which surface treatment is done to enhance the bonding between them. This procedure is repeated for the required amount of strain to be applied [39].

Bridgman proposed the HPT process in which a ring or disc shaped specimen is compressed under high pressures and torque is applied simultaneously on the specimen. Korbel et al. developed the cyclic extrusion compression (CEC) process, in which a sample is contained within a chamber and then it is extruded back and forth. Ghosh et al. developed Cyclic closed die forging (CCDF) process to produce ufg materials, in which the specimen is forged in alternate directions to get high uniform strain. Huang et al. developed repetitive corrugated and straightening (RCS) process, in which the specimen is bent with corrugated tools and then the shape is restored using straightening tools [39].

2.8 Strengthening Mechanism in UFG Materials

The strengthening mechanism of the UFG materials can be explained by Hall-Patch equation:

$$\sigma = \sigma_0 + k.d^{-0.5} \qquad (2.1)$$

The strength or hardness increases with decrease in grain size. But this equation has limitations because with decrease in grain size, strength cannot increase indefinitely. The strength cannot exceed a certain theoretical strength which is the strength of perfect whisker. In spite of this, relaxation process at grain boundaries due to extreme grain refining could lead to decrease in the strength. A region of constant strength with decreasing grain size might be expected, in the absence of grain boundary relaxation mechanism, which would be governed by fracture initiated at triple points. The hall patch relation equation (2.1), is valid only upto a certain critical value of grain size. Further refinement in grain size other weakening mechanisms such as viscous type flow, set in leads to softening of the material with decreasing grain size. The functional relation between hardness/strength and grain size for UFG materials depends upon exact deformation mechanism [40].

2.9 Fracture Toughness

It is the property of the material that is the ability of a material having crack to resist fracture. J-integral is field parameter that defines the plastic stress and stress intensity in the region around the crack tip [43]. In comparison to tensile testing, fracture toughness testing using the current ASTM standards is very expensive procedure. Also in SPD process the specimen size is limited in dimensions restricted for fracture toughness test, although many researchers attempt to find fracture toughness in UFG materials like static 3 point bend test on UFG low alloy steel fabricated by multi-pass calibre rolling at 500°C [44]. Shimokawa et al. [45] explained the fracture toughness mechanisms for UFG materials through modelling stated that GB sliding and migration is most effective in increasing fracture toughness of nano-crystalline metals with finest grains. As the grain size of the material increases, it is lattice dislocation slip that provides the principal contribution to fracture toughness enhancement.

2.10 Fracture Behaviour of Ultrafine Grained Materials

In a polycrystalline material, the crack propagates in three stages as void nucleation, void growth and finally void coalescence. The crack initiation inside the material takes place by the formation of void, which forms due to decohesion of particle or matrix interface and fracture of particle [46]. During static loading of ultrafine (UFG) and nano-crystalline (NC) grained material, the fracture occurs by dimple formation, with size much smaller as compared to coarse grained material. In some cases, the dimple size is much greater than grain size of the UFG and NC materials due to shear localization [47]. The enhanced fracture toughness is due to disclination shielding effect on the crack tip as reported by Shimokawa et al. [45]. Disclination shielding is activated in two conditions: firstly, transition of dislocation takes place from the crack tip to grain boundary and secondly, transformation of grain boundary into an energetically stable neighbouring boundary occurs when dislocations are emitted from the grain boundary [45]. Zhu et al. [48] reported that the strength and ductility of bimodal structure is sensitive to the volume fraction of the constituents and distribution of nano and micro-cracks. Das et al. [49] reported that the fracture toughness of UFG Al alloy has increased 78% as compared to coarse grained alloy due to precipitation hardening and subgrain coarsening. Hidetoshi et al. [42] reported that the improvement in fracture toughness of the ECAE processed Mg AZ31 alloy without annealing was more than the ECAE processed annealed alloy.

Chapter 3: Plan of Work

Form the literature review, as noticed that there was only a few work done on the production of ultrafine grained Magnesium ZE41 alloy and its mechanical behaviour. Hence the alloy ZE41 is selected for present dissertation work. The ultrafine grained structure was produced through the SPD route using Multiaxial Forging (MAF) and MAF followed by warm rolling. Then the tensile, fracture toughness and hardness are calculated for different conditions. The microstructural studies were carried out using Optical Microscope (OM), Transmission Electron Microscope (TEM) and Scanning Electron Microscope (SEM). The simulations were carried out for verifying the properties obtained from the experimental results using ANSYS 15.0.

Detailed plan of work stepwise is given below:

- Literature survey
- Selection of material
- Selection of process to produce the UFG material
- Experimental work
    - Hot Rolling at 490°C upto 70% reduction in two passes with 50% reduction per pass
    - Multiaxial Forging at 450°C
    - Multiaxial Forging at 450°C followed by warm rolling at 450°C.
- Experimental Testing
    - Hardness measurement
    - Tensile testing
    - Fracture toughness (3 point bend test)
- Microstructural characterisation
    - Optical Microscopy
    - Scanning Electron Microscopy (SEM)
    - Transmission Electron Microscopy (TEM)
- Simulation Work
    - Tensile testing
    - Fracture mechanics
    - Fatigue Simulations

Chapter 4: Experimental Details

4.1 Material

The magnesium alloy ZE41 used in this work was casted in-house through sand casting route followed by machining. The chemical composition of the alloy is given in the Table 4.1. Samples were cut from the casted billet and were given T5 treatment. First, the samples were placed in furnace for 2 hours at 330°C for annealing and then the samples were air cooled to room temperature. After that the samples were put in furnace for 16 hours at 180°C for solution treatment and then again cooled to room temperature in still air. The alloy then was subjected to Multi Axial Forging (MAF) and Rolling at high temperature.

4.2 Experimental Procedure

4.2.1 Multi-axial Forging

The setup for MAF consist of the following:

1. **Furnace:** The furnace was used for the heating of the samples before forging. The samples were put in the furnace for 30 minutes between two consecutive passes.
2. **Forging Die:** The forging die used for the experiments were made for die steel and shown in Fig 4.1. The die hole was having a dimension of 25mm×45mm. The stock was placed on the sample for pressing to the thickness of 20mm.
3. **Friction Screw Press:** The press was used to forge the samples at high temperature. The speed of the machine was 360 RPM and the capacity was 100 tonnes.
4. **Set of gloves** were used to handle the samples at higher temperature for safety purpose and **a pair of tong** was used to take out the samples from the furnace.

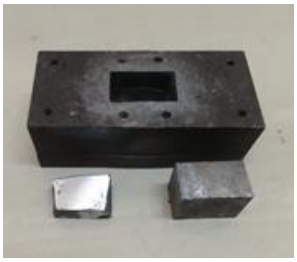

Fig. 4.1 Forging Die

For MAF, samples having dimensions of 20×25×40 mm^3 were used. The samples were forged to a cumulative strain of 2.1 and 4.2 and some samples were followed by warm rolling. Prior to

forging the samples were put in finance stabilised at 450°C for 30 min to achieve the uniform temperature of the sample. The samples were forged in a close die made of die steel. After every pass the samples were left in furnace for 30 minutes. The samples were rotated by 90° after every pass so that all the 3 axis of the sample are forged. The final dimension of the sample were same as the initial dimensions.

True strain induced per pass during forging is calculated using the formula:

$$\epsilon = \ln\left(\frac{hf}{hi}\right) \qquad (4.1)$$

Where

h_f – final height

h_i – initial height

The schematic of the forging process is as shown in Fig 4.2.

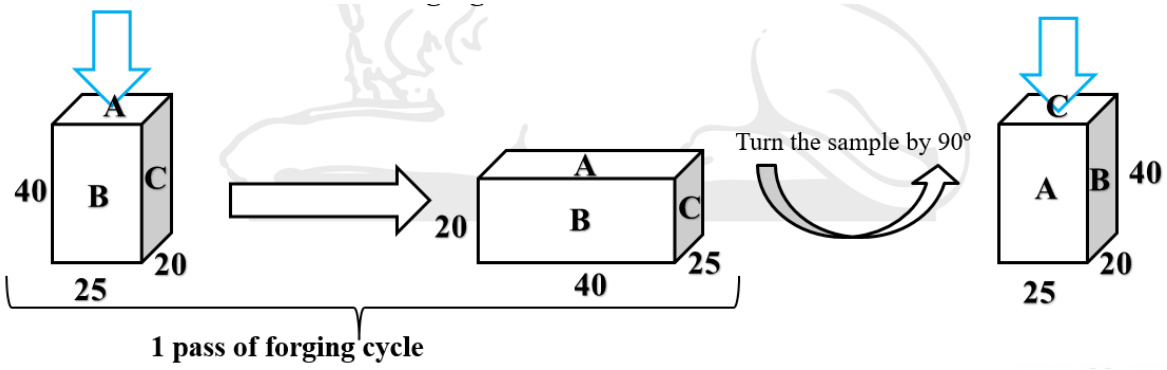

Fig. 4.2 Schematic of multiaxial forging (MAF)

True strain of nearly -0.7 is introduced in every stage of forging. Hence the total accumulated strain for 3 pass and 6 pass forged samples were 2.1 and 4.2. Just after the total number of passes were completed, the samples were quenched in cold water at room temperature to avoid any change in microstructure. After forging samples were prepared for different characterization and testing.

4.2.2 Rolling at High temperature

The roll mill used for rolling is 2 high roll mill having roll diameter of 150 mm and a speed of 8 RPM. The rolling was done for two type of samples: **1)** For Heat treated samples (Hot Rolling), **2)** For forged samples after 3 pass and 6 pass (Warm Rolling).

For Hot rolling samples were cut form the casted billet in the dimension of 10×20×30 mm^3. Large strain hot rolling was performed for better results. The reduction given per pass was about 50%, but after spring back effect the strain obtained was about 45%, hence giving total true strain of 0.6 per pass. 2 such passes were performed on the heat treated sample giving total strain of 1.2 and total reduction of 70%.

For forged samples the samples with dimension 20×25×40 mm^3 the rolling direction was chosen from the last forged direction. The total reduction given after warm rolling was 70%. The true strain was calculated using Equation (4.1).

4.3 Microstructural Characterization

4.3.1 Optical microscopy (OM)

Optical microscopy is used to see the higher resolution images of the samples. The samples as casted, heat treated, forged at different passes, forged followed by warm rolling and hot rolled samples were characterised using LEICA DM1500 M optical microscope at different magnification of 5X, 10X, 20X, 50X and 100X.

Firstly, the selected part from different condition samples was cut using diamond cutter using lubricant to avoid heating of the material. The samples were mechanically polished using SiC papers of 320, 800, 1200, 1500 and 2000 grit size. Kerosene was used to remove the polished particles form the surface. After that mechanically polished samples were finally polished on a disc polisher on synthetic medium nap-cloth of 2µm size using diamond paste. The cloth polished samples were than etched for 3 seconds in the solution of 2.5ml acetic acid, 3g picric acid, 50 ml ethanol and 5 ml distilled water.

4.3.2 Scanning Electron Microscopy (SEM)

The Carl Zeiss EVO18® SEM with LaB6 filament was used for the fractrography of the fractured tensile test samples. The fracture surface of tensile test samples of different condition processed samples were examined using SEM. Any sample preparation is not necessary for fractrography analysis.

4.3.3 Transmission Electron Microscopy (TEM)

The transmission electron microscope was used for the examination of internal features of the as-cast and processed samples. The samples for TEM were first ground to the thickness of 0.1mm

using SiC paper and then the disc of 3mm dia were punched out from the grounded plate specimen. The discs were finally electropolished using a Twin Jet polisher in a solution containing 90% acetic acid and 10% perchloric acid at 20 volts. After electro-polishing the disc were dipped in a nitric acid dilute solution for 1 or 2 seconds. After that these disc were cleaned in ethanol.

4.4 Mechanical Testing

4.4.1 Hardness Testing

Hardness is a material property which is able to counterattack plastic deformation mostly by penetration or scratch. In Vickers micro hardness tester, both the soft and hard materials can be tested. It has a diamond indenter having pyramid shape with a load range upto 30 kgf. This is a very simple method for finding out the hardness of the specimen.

The hardness values for of different processed samples were evaluated using FIE Vickers Hardness testing machine. The samples for hardness testing were prepared for good surface finish so the values obtained have a satisfactory level of accuracy. The samples were mechanically polished using SiC papers of grit size 320, 800, 1200 and 1500, and finally cloth polished using a diamond paste on a disc polisher using synthetic medium nap-cloth of 2μm size. Atleast 10 readings were taken from each and every sample for good level of accuracy in results.

4.4.2 Universal Testing Machine

Uniaxial tensile tests and 3 point bend tests were carried out on the S- series, H25K- S Universal testing machine. Tensile test were carried out at crosshead speed of 1 mm/min to evaluate the yield strength, ultimate tensile strength and elongation to failure. The tensile test samples were prepared having gauge length of 10mm, width of 2 mm and thickness of 2 mm, the ratio of length to square root of cross-section area is maintained as per ASTM standards.

Fracture toughness evaluation was carried out with crosshead speed of 3mm/min on chevron notch 3 point bend specimen as shown in Fig 4.3. The 3 point bend specimen prepared was having span length (L) of 30 mm, thickness (B) of 3.5 mm and a width (W) of 7 mm. The depth of notch and precrack (a) was 3.85 mm, the ratio of a/W maintained 0.55.

Generally, fracture toughness for ductile materials is assessed using J-Integral measurements by applying a multiple specimen test procedure. In this experiment fracture energy is calculated as

per ASTM 1820E basic test method. Atleast 3 test samples were tested from every processing condition for required accuracy.

Fig. 4.3 3-Point Bend sample for fracture toughness testing

The fracture toughness for the brittle fracture is assessed by evaluating the stress intensity factor (K_{IC}). Linear elastic fracture mechanics is used for brittle materials as there is no plastic deformation occurs while fracture. The stress intensity factor of the alloy after and before processing was calculated from the 3-point bend test and using the formula proposed by Xian et al. [59]. The stress intensity factor under mode I is calculated using:

$$K_Q = \frac{P_Q}{B\sqrt{W}} f(a/W) \qquad (4.2)$$

Where $f(a/W)$ is a geometry function that depends on the crack size to the specimen width ratio a/W only. For 3-point bend specimen

$$f\left(\frac{a}{W}\right) = \frac{3\frac{s}{W}\sqrt{\frac{a}{W}}}{2\left(1+2\frac{a}{W}\right)\left(1-\frac{a}{W}\right)^{3/2}}\left[1.99 - \frac{a}{W}\left(1-\frac{a}{W}\right)\left\{2.15 - 3.93\left(\frac{a}{W}\right) + 2.7\left(\frac{a}{W}\right)^2\right\}\right] \qquad (4.3)$$

Where a= crack length

W= width of the 3-point bend specimen

B= thickness of the sample

s= span length of the sample

P_Q= maximum load for the initial elastic loading.

Validation of fracture toughness:

For K_Q to be a valid K_{IC} the following conditions must be satisfied [56].

$$B, a \geq 2.5\left(\frac{K_Q}{\sigma_{ys}}\right)^2$$

$$P_{max} \leq 1.1P_Q$$

But in our case this condition is not able to satisfy because the B comes out to be in the range of 15mm to 25mm while our B is equal to 3.5mm. And making sample of this much thickness is not possible in this study. So ASTM Standard E1820-11[57] provides and alternative technique to determine K_{JC} i.e. fracture toughness at crack initiation point.

According to this standard the K_{JC} can be obtained using the formula [57]

$$K_{JC} = \sqrt{\frac{EJ_C}{(1-\vartheta^2)}} \qquad (4.4)$$

where J_c can be obtained using

$$J = \left(\frac{1+\alpha}{1+\alpha^2}\right) \times \frac{2A_{tot}}{Bb} \qquad (4.5)$$

where b=W-a,

α is constant determined by $\alpha = 2\sqrt{\left(\frac{a}{b}\right)^2 + \frac{a}{b} + \frac{1}{2}} - 2\left(\frac{a}{b} + \frac{1}{2}\right)$

and A_{tot} is the area under the force extension curve determine by 3 point bend test.

Chapter 5: Finite Element Simulations

5.1 Introduction

Finite Element Analysis (FEA) simulation is a way of predicting and optimizing the behaviour of various objects/systems that are often connected without relying on the physical existing models, measurements or prototypes. The system is numerically divided into a very large number of finite volumes called “elements”. This process is meshing, the better the mesh, the better is the physical representation of model. The primary use of this finite element is to connect nodes with predictable mathematical equations based on stiffness between the nodes. The type of element used is often selected according to the problem statement [26]. The behaviour of each element is understood by this stiffness matrix. By combining the behaviour of every element using simultaneous equations, the overall behaviour of the physical model is predicted.

5.2 FEA Software Package

- ALGOR
- ANSYS
- COSMOSL
- STARDYNE
- NASTRAN
- SAP90
- ADINA
- ABAQUS, etc.6

5.3 How FEA Works:

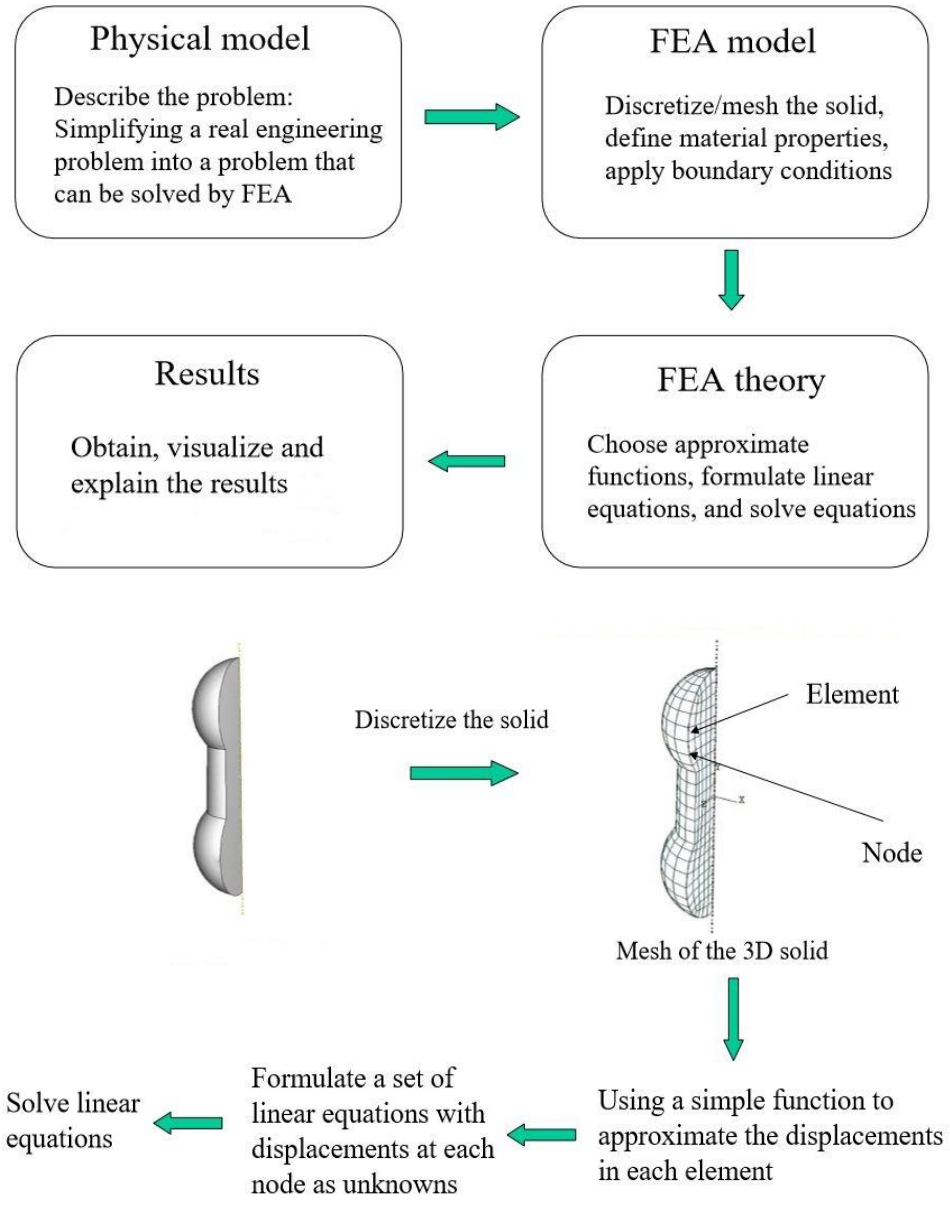

Fig.5.1 Schematic of Working Method of Finite Element Analysis [30]

5.4 ANSYS

ANSYS is a finite element analysis program used in this work for simulating the fracture mechanics problem. It has many FEA capabilities, ranging from a simple, linear, static analysis to a complex, non-linear, transient dynamic analysis.

5.5 Fracture Mechanics

Cracks or flaws exists in most of the structures and machine components because of many reasons. The material may be defective, cracks may be introduced in it either in manufacturing processes or may be in service due to environmental conditions. The presence of such irregularities in the microstructure of the material can significantly affect the component's life and integrity under the action of applied mechanical loads or environmental conditions [51].

5.5.1 Fracture

Typically, fracture analysis is carried out using either the stress intensity factor (SIF) or the energy criterion. In energy release rate criterion, the energy required for a unit extension of the crack characterizes the fracture toughness. In stress intensity factor (SIF) approach the critical value of the amplitude of the deformation and stress field characterizes the fracture toughness. Under some conditions both criteria are equivalent.

Depending upon the failure kinematics there are 3 modes of fracture. In any material either of the modes exists or any combination can occur.

Mode I- opening/tensile mode

Mode II- Shearing/sliding mode

Mode III- Tearing/out of plane mode.

Typically in fracture mechanics either the energy release rate or the amplitude of stress and deformation fields at crack tip is described.

5.5.2 Fracture mechanics parameter calculation

The following parameters are most common in any fracture mechanics analysis:

- J-integral
- Energy Release Rate
- Stress Intensity factor
- T- stress
- Material force

5.5.2.1 J-integral

J-Integral is one of the most widely used fracture mechanics parameter for linear plastic and nonlinear elastic-plastic materials. The J-Integral is defined as follows [33]:

$$J = \lim_{\Gamma \to 0} \int_{\Gamma_0} \left[(w + T)\delta_{ij} - \sigma_{ij} \frac{\partial u_j}{\partial x_I} \right] n_i d\Gamma \qquad (5.1)$$

Where

w- strain energy density,

T- the kinematic energy density,

σ- stress,

u- displacement vector, and

Γ- contour over which the integration is carried out.

Hutchinson [52] and Rice [33] and Rosengren [53] showed that the J-Integral as the crack-tip field in any nonlinear elastic material. They all assumed a power law relationship between plastic strain and stress. If elastic strain is present, the relationship for uniaxial deformation is given as:

$$\frac{\varepsilon}{\varepsilon_0} = \frac{\sigma}{\sigma_0} + \alpha \left(\frac{\sigma}{\sigma_0} \right)^n \qquad (5.2)$$

Where

σ_0- yield stress of the material, and

$\varepsilon_0 = \sigma_0 / E$,

α- a dimensionless constant, and n is the hardening component. The crack-tip stress and strain ahead of crack tip can be expressed as:

$$\sigma_{ij} = f(\theta) \left(\frac{J}{r} \right)^{\frac{1}{n}} \qquad (5.3)$$

And

$$\varepsilon_{ij} = g(\theta) \left(\frac{J}{r} \right)^{\frac{n}{n+1}} \qquad (5.4)$$

For elastic material, n = 1 and the above equation showed the $1/\sqrt{r}$ singularity.

5.5.2.2 Stress Intensity Factor

It is limited to linear elastic material only and the stress and strain fields near crack tip expressed as:

$$\sigma_{ij} = -\frac{K}{\sqrt{r}} f_{ij}(\theta) \qquad (5.7)$$

$$\epsilon_{ij} = -\frac{K}{\sqrt{r}} g_{ij}(\theta) \qquad (5.8)$$

Where K is the stress-intensity factor, r and θ are coordinates of a polar coordinate system (Fig. 5.3). These equations can be applied to any of the three fracture modes.

For a Mode I crack, the stress field is given as:

$$\sigma_x = \frac{K_I}{\sqrt{2\pi r}} cos\left(\frac{\theta}{2}\right)\left(1 - sin\left(\frac{\theta}{2}\right) sin\left(\frac{3\theta}{2}\right)\right) \qquad (5.9)$$

$$\sigma_y = \frac{K_I}{\sqrt{2\pi r}} cos\left(\frac{\theta}{2}\right)\left(1 + sin\left(\frac{\theta}{2}\right) sin\left(\frac{3\theta}{2}\right)\right) \qquad (5.10)$$

$$\sigma_{xy} = \frac{K_I}{\sqrt{2\pi r}} cos\left(\frac{\theta}{2}\right) sin\left(\frac{\theta}{2}\right) cos\left(\frac{3\theta}{2}\right) \qquad (5.11)$$

5.6 Fatigue Simulations

Fatigue testing is a mechanism in which a structure is applied with repetitive loading with different amplitude and stress ratios for the material to fracture. In fatigue loading the material fractures at a load level much lesser that the ultimate strength of the material.

The main factors that contributes to the failure of material due to fatigue loading includes:

- Number of cycles applied
- Amplitude of the stress applied
- Mean value of the alternating stress applied
- Presence of any internal flaws or points of stress concentration.

The fatigue calculations are based on the ASME Boiler and Pressure Vessel Code, Section III and section VIII division 2 [51] for guidelines on the simplified elastic plastic adaptations, range counting and cumulative fatigue addition by Miner's Rule.

As noted earlier, fatigue is due to repetitive loading:

When minimum and maximum stress levels are constant, this is referred to as constant amplitude loading. This is a much more simple case and will be discussed first. Otherwise, the loading is known as variable amplitude or non-constant amplitude and requires special treatment.

The basic procedure of the stress life based fatigue analysis is as follows:

Performing a fatigue analysis is based on a linear static analysis. Fatigue analysis is automatically performed by Simulation after a linear static solution. It does not matter whether the Fatigue Tool is added prior to or after a solution since fatigue calculations are performed independently of the stress analysis calculations. Although fatigue is related to cyclic or repetitive loading, the results used are based on linear static, not harmonic analysis. Also, although nonlinearities may be present in the model, this must be handled with caution because a fatigue analysis assumes linear behavior. As with a linear static analysis, Young's Modulus and Poisson's Ratio are required material properties. If inertial loads are present, mass density is required, if thermal loads are present, thermal expansion coefficient and thermal conductivity are required, if a Stress Tool result is used, Stress Limits data is needed. This data is also used for fatigue for mean stress correction. The Fatigue Module also requires S-N curve data in the material properties of the Engineering Data. The type of data is specified under "Life Data". The S-N curve data is input in "Alternating Stress vs. Cycles". If S-N curve material data is available for different mean stresses or stress ratios, these multiple S-N curves may also be input.

The Goodman theory is suitable for low-ductility metals. No correction is done for compressive mean stresses.

The Soderberg theory tends to be more conservative than Goodman and is sometimes used for brittle materials.

The Gerber theory provides good fit for ductile metals for tensile mean stresses, although it incorrectly predicts a harmful effect of compressive mean stresses.

Chapter 6: Result and Discussion

In this chapter, the results obtained from mechanical and fracture testing of ultrafine grained Magnesium alloy ZE41 processed using Multi-axial Forging (MAF) and MAF followed by warm rolling are deliberated. The present research work was concentrated on various experimental studies of the alloy such as: (i) Mechanical behaviour and microstructural analysis of Mg ZE41 alloy processed via MAF and MAF + warm rolling: (ii) effect of number of passes of forging on the properties and microstructure of the alloy; (iii) fracture behaviour of the alloy via 3 point bend test and fractrography. The results of each study are demonstrated using detailed microstructural characterization of the samples under different conditions.

6.1 Experimental Results

6.1.1 Chemical Composition

The chemical composition of the casted billet of the alloy is as shown in table 6.1

Table 6.1 Chemical composition of ZE41 Mg alloy

Alloying Element	Standard Composition (weight %)	Obtained (weight %)
Zinc	3.5 - 5.0	4.45
Zirconium	0.4-1.0	0.55
Total rare earth	0.8 – 1.70	1.2
Manganese	0.15 Max	0.004
Iron	0.01 Max	0.002
Copper	0.03 Max	0.005
Nickel	0.005 Max	0.002
Silicon	0.01 Max	0.007
Magnesium	Remainder	Remainder

6.1.2 Mechanical Properties

6.1.2.1 Vickers Hardness

The hardness values of the as cast, T5 treated, 3 pass and 6 pass forged, 3 pass followed by warm rolling and 6 pass followed by warm rolling, with and without heat treatment is as shown in table 6.2. The comparison between the heat treated (HT) and non-heat treated (NHT) samples is also represented graphically in Fig. 6.1. As shown in the table 6.2, the hardness values for the as casted alloy is 65 HV. This value increased to 85 for 70% rolled sample at 450ºC. The values are nearly close to each other for every processing condition and vary only by small amount, this can be attributed to the fact that all the workings are at high temperatures of nearly 450ºC. The improvement in harness can be attributed to higher dislocation density in the forged and forged + warm rolled samples. Also with the grain refinement, the mobility of dislocation can be pinned down by low angle grain boundaries and high angle grain boundaries that might be the reason to high hardness in 3 pass forged sample. The small decrease in hardness may be attributed to the softening affect occurred due to large strain in the material. The results are in good agreement with Ding R. et al. [12] and Aibin Ma at al. [13]. The lowering in hardness after rolling in the forged samples may be due to the softening at large strain due to the effect of dynamic recrystallization [12].

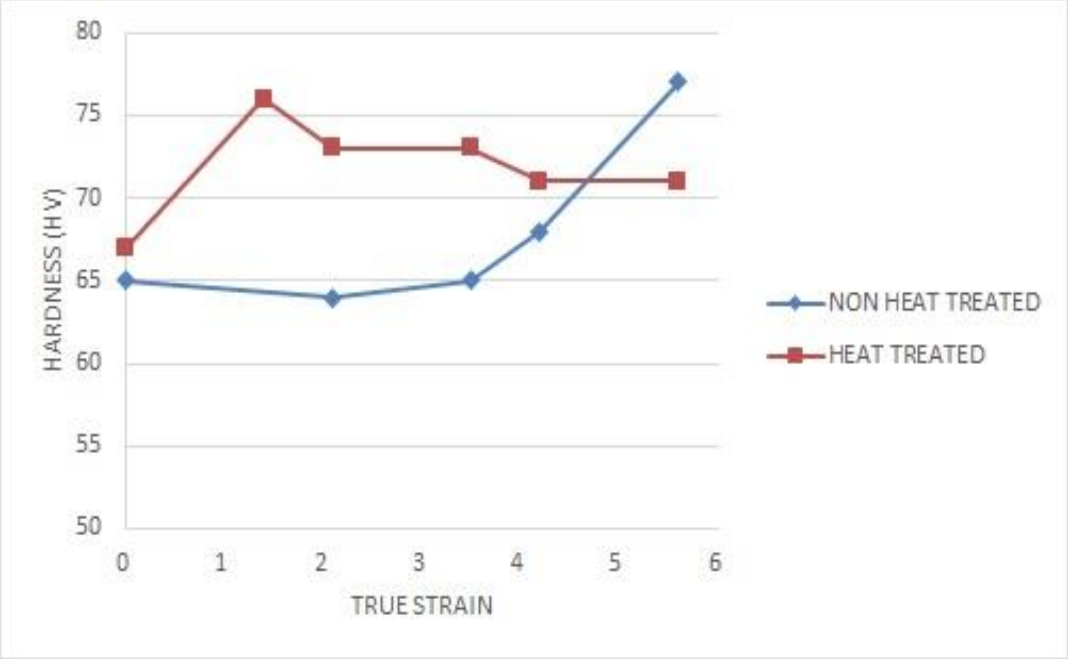

Fig. 6.1 Vickers Hardness for Non Heat Treated (NHT) and Heat Treated (HT) samples

Table 6.2 Vickers Hardness at different conditions.

Condition of Processing	Hardness (HV5)
As cast	65
T5 treated	67
70% rolling at 490°C	76
3 pass forging (NHT)	64
3 pass forging + 70% rolled (NHT)	65
6 pass forged (NHT)	68
6 pass forged + 70% rolled (NHT)	77
3 pass forged (HT)	73
3 pass forged + 70% rolled (HT)	73
6 pass forged (HT)	71
6 pass forged + 70% rolled (HT)	71

6.1.2.2 Tensile Strength

Tensile strength and elongation to failure of the magnesium ZE41 alloy processed as different conditions is shown in Fig. 6.2, 6.3 and 6.4. The summarized yield strength, ultimate strength and elongation at fracture is represented in Table 6.2.

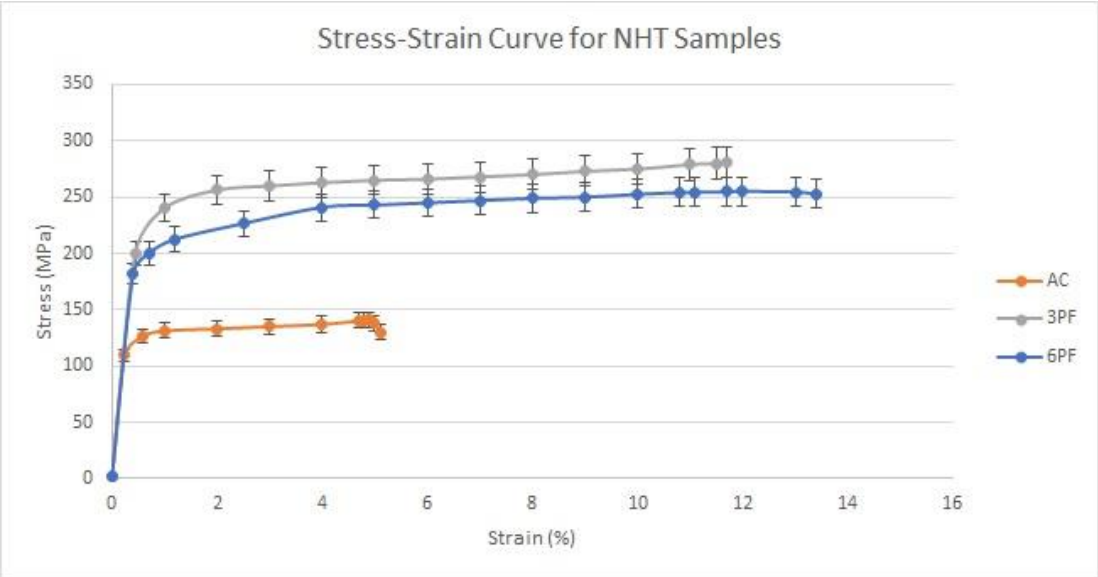

Fig. 6.2 Stress- Strain Curve for Non-Heat Treated Samples

Fig. 6.2 shows the stress strain curve for the non-heat treated (NHT) samples as casted, forged to 3 passes (3PF) and 6 passes (6PF). It predicts that there is increase in both tensile strength and elongation at failure. The ultimate strength obtained of the as casted sample was 141 MPa. The maximum ultimate strength that is 282 MPa was achieved after 3 passes of forging which again decreases to 255 MPa after 6 passes of forging. There is 100% increase in strength after 3PF and about 80% increase after 6PF. The elongation to failure for the as casted sample was recorded as only 5.15%. The elongation to failure after 3PF was recorded 11.7% and after 6PF it further increases to 13.4%. There is 127% increase in ductility after 3PF and 160% increase after 6PF. Here it can be seen clearly that the strength after 3 passes of forging is more than 6 passes of forging, but the ductility increases further upto 6 passes. This decrease in strength and increase in ductility can be explained by the fact that the softening effect is observed if we increase the strain beyond a certain point. The results obtained here are in good agreement with Figueiredo et al. [11], suggesting that there the better properties are attained at lesser strain and further increasing strain increase the grain size and hence ductility is improved further with the loss of strength.

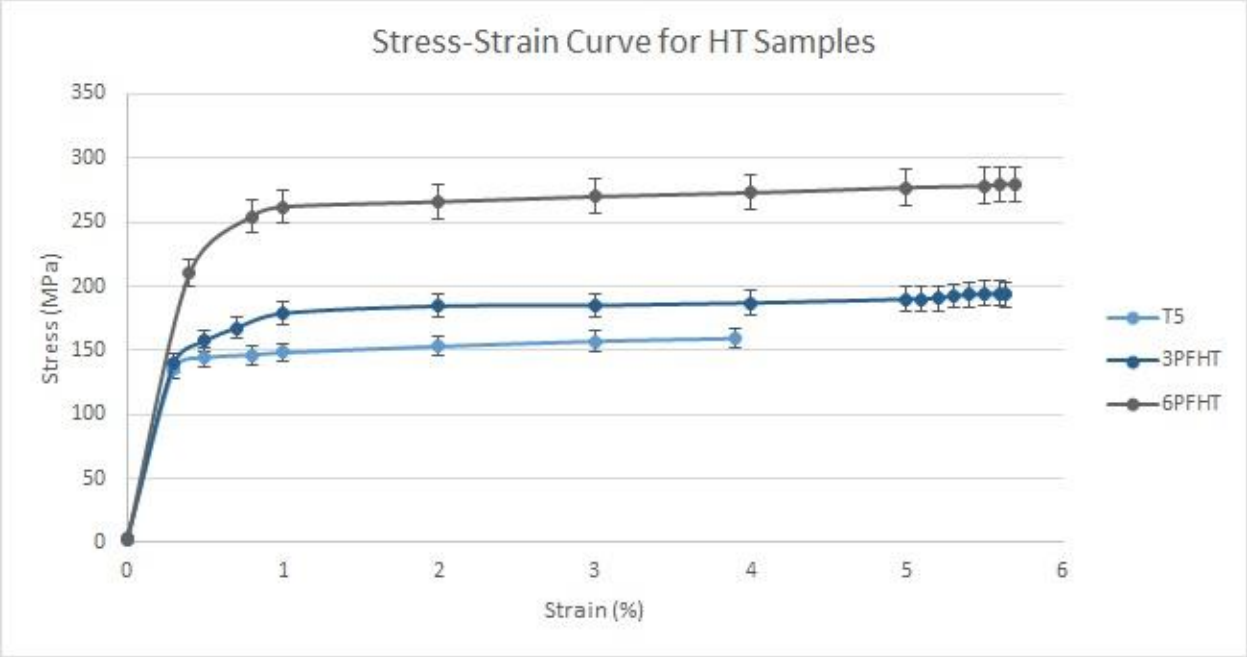

Fig. 6.3 Stress- Strain Curve for Heat Treated (HT) Samples

Fig 6.3 shows the stress strain curve for the T5 Heat treated samples at different conditions of processing. The initial strength of the T5 treated alloy was 160 MPa and elongation to failure is 4%. There is increase in both strength and elongation to failure after 3 pass forging (3PF) and 6

pass forging (6PF). The strength increases to 200 MPa after 3PF and 280 MPa after 6PF. The elongation after both 3PF and 6PF is nearly same about 6%. It can be shown here that there is not much grain refinement in the heat treated samples after 3 pass and even 6 passes of forging as compared to the non-heat treated samples. There is only 25% increase in strength after 3PF and about 75% increase after 6PF. The increase in elongation to failure is only 50% after both 3PF and 6PF. This type of behaviour is due to the fact that after T5 treatment of the alloy the stress at the grains are released and they get bigger in size. Hence there is large amount of strain is required for better strength and ductility. The strength is increasing with increasing number of cycles suggesting that for heat treated condition as the initial grain size is more the larger strain is required to obtain a fine microstructure. The mechanism of the grain refinement is dynamic recrystallization [16], because the working temperature is higher than half the melting point temperature.

Fig 6.4 shows the stress strain curve for rolling from different initial condition specimens. There is a large increase in the strength and ductility after rolling from each condition. The strength obtained after 70% rolling after T5 treatment was 315 MPa and elongation to failure was 13.5%. The T5 treated samples rolled after 3 passes and 6 passes of forging showed a tensile strength of 325 MPa and 315 MPa respectively and the elongation to failure obtained was 15% and 17% respectively. The non-heat treated samples showed lower strength and ductility compared with heat treated samples. The non-heat treated samples after 3 passes and 6 passes of forging showed a tensile strength of 295 MPa and 280 MPa respectively and elongation to failure of 15.2% and 12%. This variation in strength and ductility of heat treated and non-heat treated samples id due to the initial microstructure of alloy. The deformation mechanism is also different for both the conditions.

By comparing results from all the conditions of deformation, it can be found that the best strength and ductility is given by forged + warm rolled samples after T5 heat treatment. As magnesium is a brittle material, it does not show any yielding before failure, hence the yield point can be calculated using 0.2% proof strain. The increase in both ductility and strength is in agreement with the results obtained by Aibin Ma et al. [13] using ECAP.

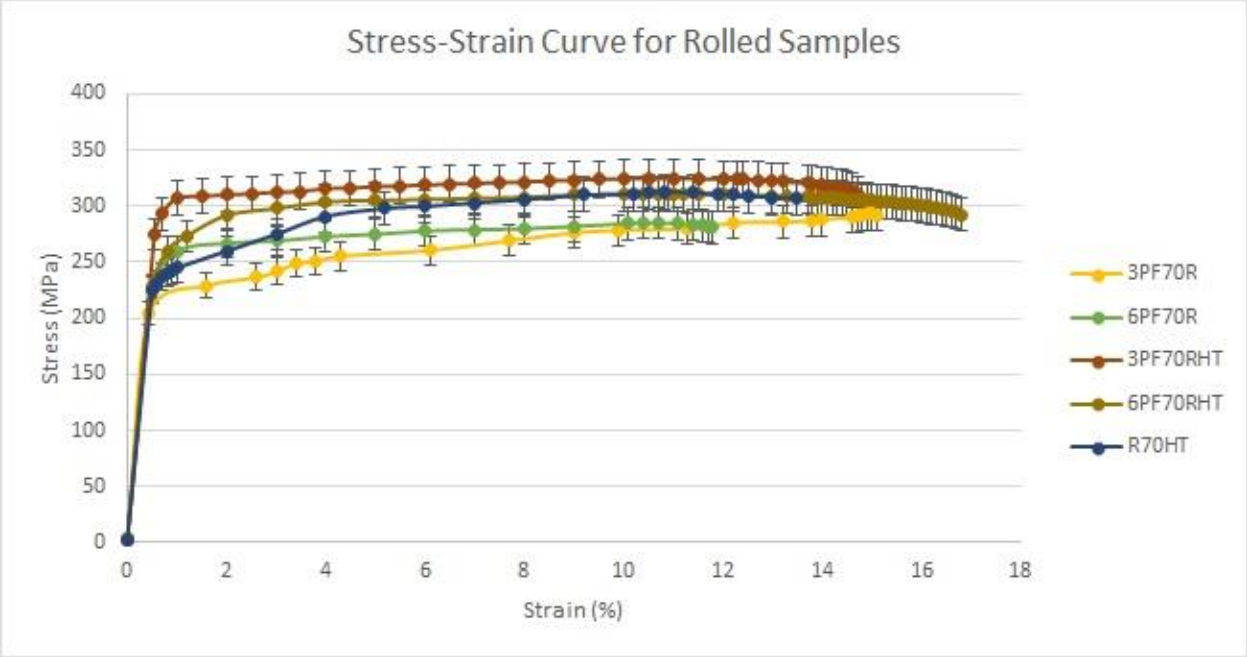

Fig. 6.4 Stress- Strain Curve for Samples Rolled from Different Initial Conditions.

Table 6.2 Strength and Ductility of different condition processed samples.

S. No.	Condition	Yield Strength (MPa)	Ultimate Tensile Strength (MPa)	Maximum Elongation (%)
1	As Cast	118	141	5.2
2	T5 Heat Treated	137	160	4
3	70% Rolled (HT)	230	315	13.5
4	3 PF (HT)	146	200	6
5	3 PF + 70% Rolled (HT)	285	325	15
6	6 PF (HT)	225	280	6
7	6 PF + 70% Rolled (HT)	250	315	17
8	3 PF (NHT)	215	282	11.7
9	3 PF + 70% Rolled (NHT)	230	295	15.2
10	6 PF (NHT)	200	255	13.4
11	6 PF + 70% Rolled (NHT)	235	280	12

6.1.2.3 Fracture Toughness

Fracture toughness of the material with different processing conditions is reported in terms of Stress Intensity Factor (K_{JC}) and J-integral calculations from the 3-point bend test results. The method for determination of J_C and K_{JC} is explained in section 4.4.2.

6.1.2.3.1 J-integral

The fracture energy (J-integral) for different conditions is presented in Table 5.3. It can be clearly visible that the fracture energy increases for the material in not heat treated condition for 3 pass forging and then decreases a little for 6 passes of forging. But for heat treated material the fracture energy decrease for both 3 pass forged and 6 pass forged specimen, but here 6 pass forged sample have more fracture toughness than 3 pass forged sample. These results are in quite good agreement with the tensile results discussed in previous section. Hidetoshi et al [41] established that the fracture toughness of magnesium alloys increases with decreasing grain size. The results obtained here are in good agreement with their observation. For NHT condition alloys, as there is grain refinement in 3 passes, the strength increase due to the dislocation pile up at grain boundaries, which restricts the crack propagation. By increasing the number of passes to 6 the dislocations are more and more accumulated and the dislocations get embedded in the grains of the material, giving way to crack to propagate. For HT condition samples, the fracture toughness decreases first for 3 pass forged sample, because for heat treated condition there are stress free grains and it takes large strain to get fine grains. After 6 passes of HT condition sample the fracture toughness increase and it is more than that of initial T5 treated condition.

There is increase in fracture toughness after rolling after every condition for HT samples. But there is drastic reduction in fracture toughness after the rolling in 3 pass forged NHT sample. This attributed to the fact that with increasing strain after 3 pass of forging for NHT conditions the fracture toughness is decreased. But for HT samples the fracture toughness is increased after rolling for both 3 pass and 6 pass forged samples.

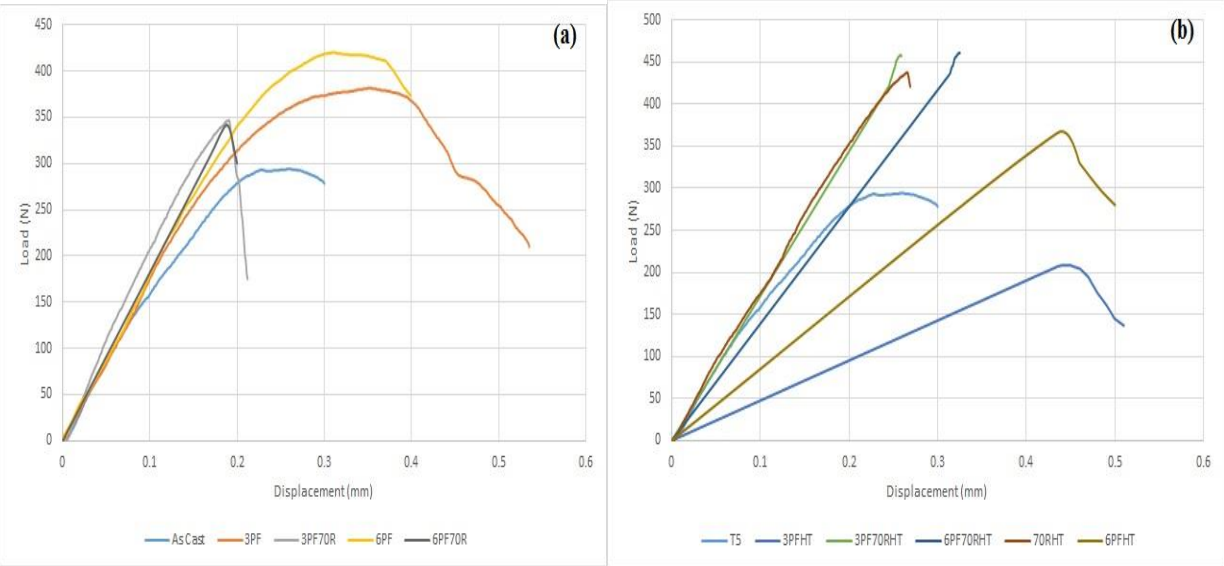

Fig. 6.5 Load-Displacement Curve obtained from 3-point bend test, (a) Non-Heat Treated samples, (b) Heat Treated Samples

Table 6.4 J-Integral (J_{IC}) values calculated from 3-point bend test for different condition processed samples.

S. No.	**Processing Condition**	**J-Integral, J_{IC} (kJ/m^2)**
1	As Cast	8
2	T5	7.6
3	3PF	16.5
4	3 PF70R	7.3
5	6PF	14.7
6	6PF70R	6.6
7	3PFHT	5.1
8	3PF70RHT	10.1
9	6PFHT	10.8
10	6PF70RHT	12.5
11	70RHT	12.7

6.1.2.3.2 Stress Intensity Factor

Stress intensity factor (SIF) is widely used to represent the fracture toughness of the brittle materials. It is mostly used for the linear elastic fracture analysis of the material. Stress intensity factors for different processed samples are represented in Table 6.4. The K_{JC} values are calculated from the 3-point bend test using equation 4.4. The K_{JC} value showed a clear improvement for the processed samples after forging followed by rolling. The value of K_{JC} showed an increment of more than 50% after 3 pass and 6 pass forging followed by rolling. The large strain hot rolled sample also showed a marked improvement in the K_{JC} value. The results showed that the crack arrest capability of the material has increased with increasing deformation strain on the material.

Table 6.5 Stress Intensity Factor (K_{JC}) values calculated from 3-point bend test for different condition processed samples.

S. No.	Processing Condition	Stress Intensity Factor, K_{JC} (MPa.$\sqrt{m}$)
1	As Cast	15.2
2	T5	16.0
3	3PF	30.5
4	3 PF70R	16.9
5	6PF	27.6
6	6PF70R	17.1
7	3PFHT	12.4
8	3PF70RHT	24.1
9	6PFHT	24.3
10	6PF70RHT	26.5
11	70RHT	28.7

6.1.3 Microstructural Characterization

6.1.3.1 Optical Microstructure Analysis

Fig 6.6 shows the optical microstructure of the alloy as casted and after different processing routes. The as casted samples Fig. 6.6 (a) shows that the initial grain size is about 150µm. As it can be shown through the optical micrographs, there is gaps between grains of as casted alloy Fig. 5.6 (a), but after processing the gap is suppressed Fig. 6.6 (b), (c) and (d). The grains are elongated in the rolling direction as is shown in Fig. 6.6 (c). The grains are totally broken after 6 pass of forging and the dynamic recrystallization started at the grain boundaries as shown in Fig.6.6 (b). After 6 passes of forging, fig 6.6 (d), there is large number of dislocations agglomerated, that can be the reason for the high strength but low ductility of the 6 pass forged sample.

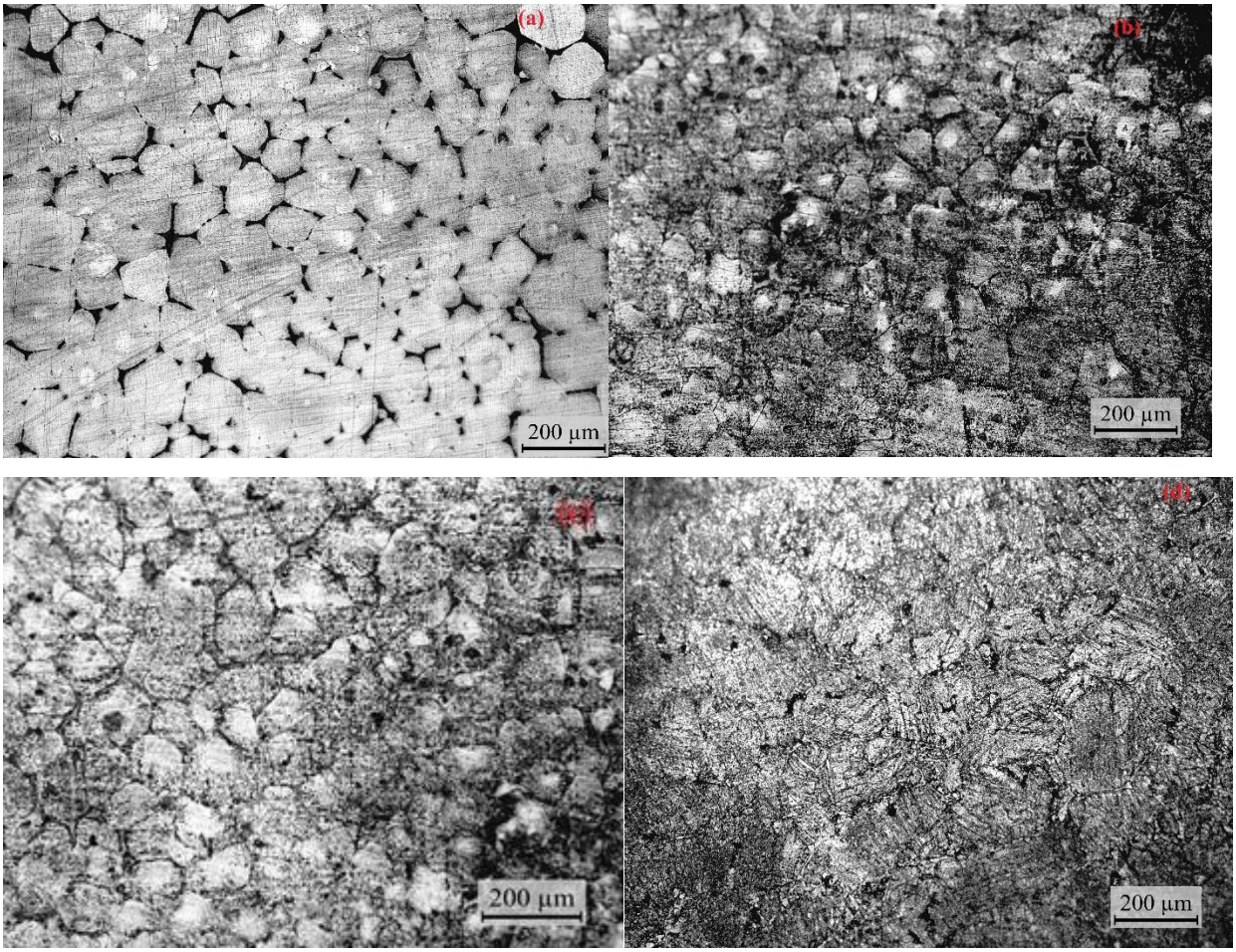

Fig. 6.6 Optical micrographs of Magnesium ZE41 alloy (a) as received, (b) 3 pass forged, (c) 70% rolled, (d) 6 pass forged.

6.1.3.2 TEM Observations

TEM was used to find out the grain size and deformation mechanism at the sub-micron level. The TEM images for 6PFHT, 6PF70RHT, 3PF70RHT and R70HT samples are shown in Fig. 6.7 (a)-(d). The 6PFHT alloy possessed an ultrafine grain microstructure with grain size of nearly 0.7µm Fig. 6.7 (b). The 3PF70RHT alloy was having ultrafine grain microstructure of with nearly 0.9-1µm Fig. 6.7 (c). The dislocation cells are clearly visible in the 70RHT sample, which increases the strength and ductility of the material Fig. 6.7 (d). The fine grain microstructure is obtained in 70RHT sample because the Large Strain Hot Rolling (LSHR) was applied instead of normal rolling. The grain size has increased by rolling on the 6-pass forged sample because of dynamic recovery process. The newly developed subgrain is also seen in the alloy (shown by white arrow).

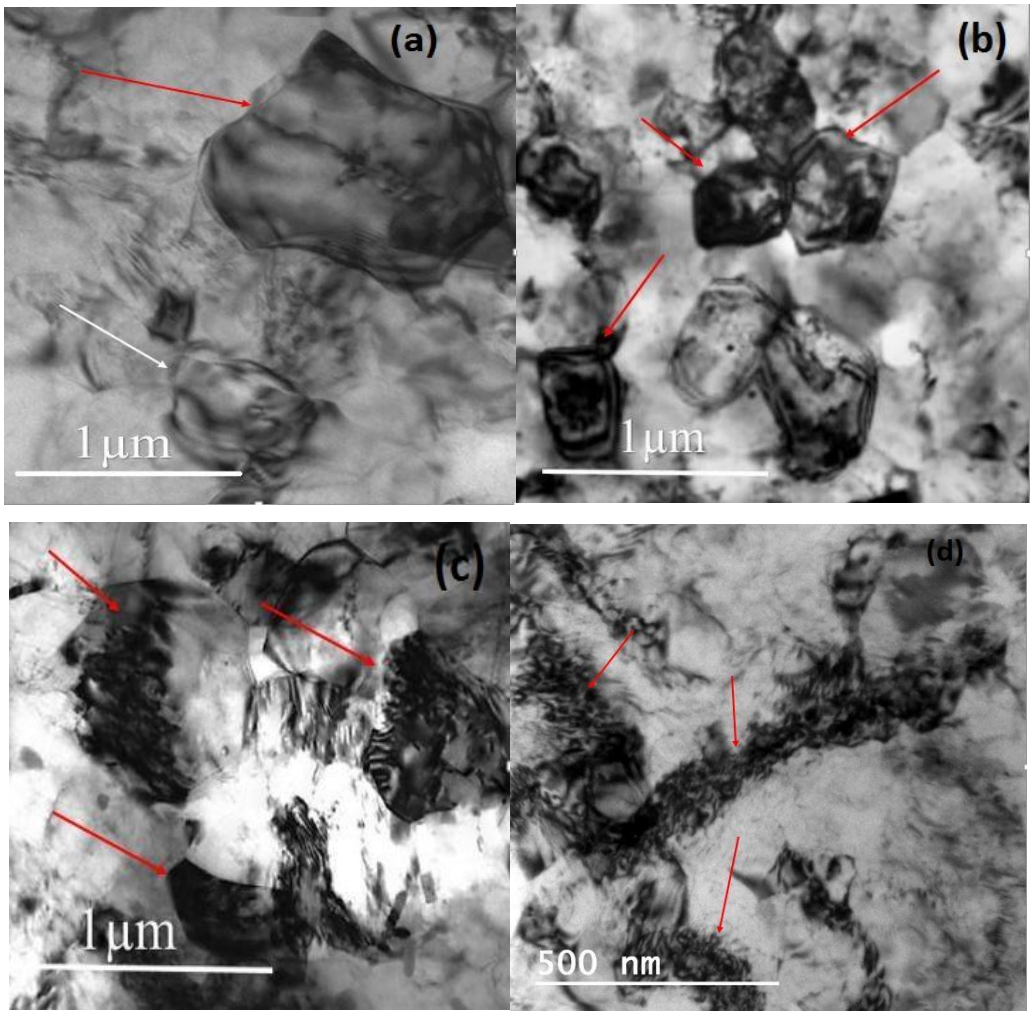

Fig. 6.7 TEM images of the processed sample (a) 6PF70RHT sample, (b) 6PF sample, (c) 3PF70RHT sample, (d) R70HT sample.

6.1.3.3 Fractrography

The fractrography of the broken samples after tensile test are as shown in this section. The fracture surface images of tensile test of as casted, 3 pass forged, 3 pass forged + 70% rolled, 6 pass forged, 6 pass + 70% rolled and 70% rolled sample after heat treatment is as shown in Fig. 6.8. The micro-cracks were initiated from the grain boundary T-phase. The intergranular fracture was observed in the as cast sample Fig. 6.8 (a), there was no evidence of significant plastic deformation in the as cast alloy. Some tearing ridges were also observed on the fracture surface, shown by red arrow, which corresponds to local deformation at grain boundaries without T-phase. After MAF, the fracture surface consisted of both cleavage planes (shown by white arrow) and tearing ridged, Fig 6.8 (b), (d). The average size of the cleavage plane decreases from 3 pass to 6 pass forging and therefore with the decrease in particle and grain size. It can be seen from Fig. 6.8 (d), the fracture surface of 6 pass MAF formed alloy was composed of a large number of dimples and tear ridges, which indicated the occurrence of significant plastic deformation.

The fracture surface images of the tensile tested rolled specimens with different initial conditions is as shown in Fig 6.8 (c), (d) and (e). The fracture surface is dimpled with elongated structure due to rolling. The mode of fracture is cleavage fracture, shown by arrows. For 70% rolled sample there are both cleavage and tear ridges, but the tear ridges goes on decreasing with increasing strain imposed by processing, hence by reduction in grain and particle size. There are clearly visible dimpled fracture and tear ridges shown by arrow, Fig. 6.8 (c), (e), showing enough evidence of plastic deformation and grain size reduction. The fracture surface for as cast and 3 pass forged samples were somewhat similar to each other showing crack produced through the triple junction of the grain boundaries. A very tiny amount of grain boundary sliding was observed in the 3 pass forged sample. The samples with higher strain showed clear evidence of grain boundary sliding. This observation shows that the main deformation mechanism in the ultrafine grained alloy was grain boundary sliding.

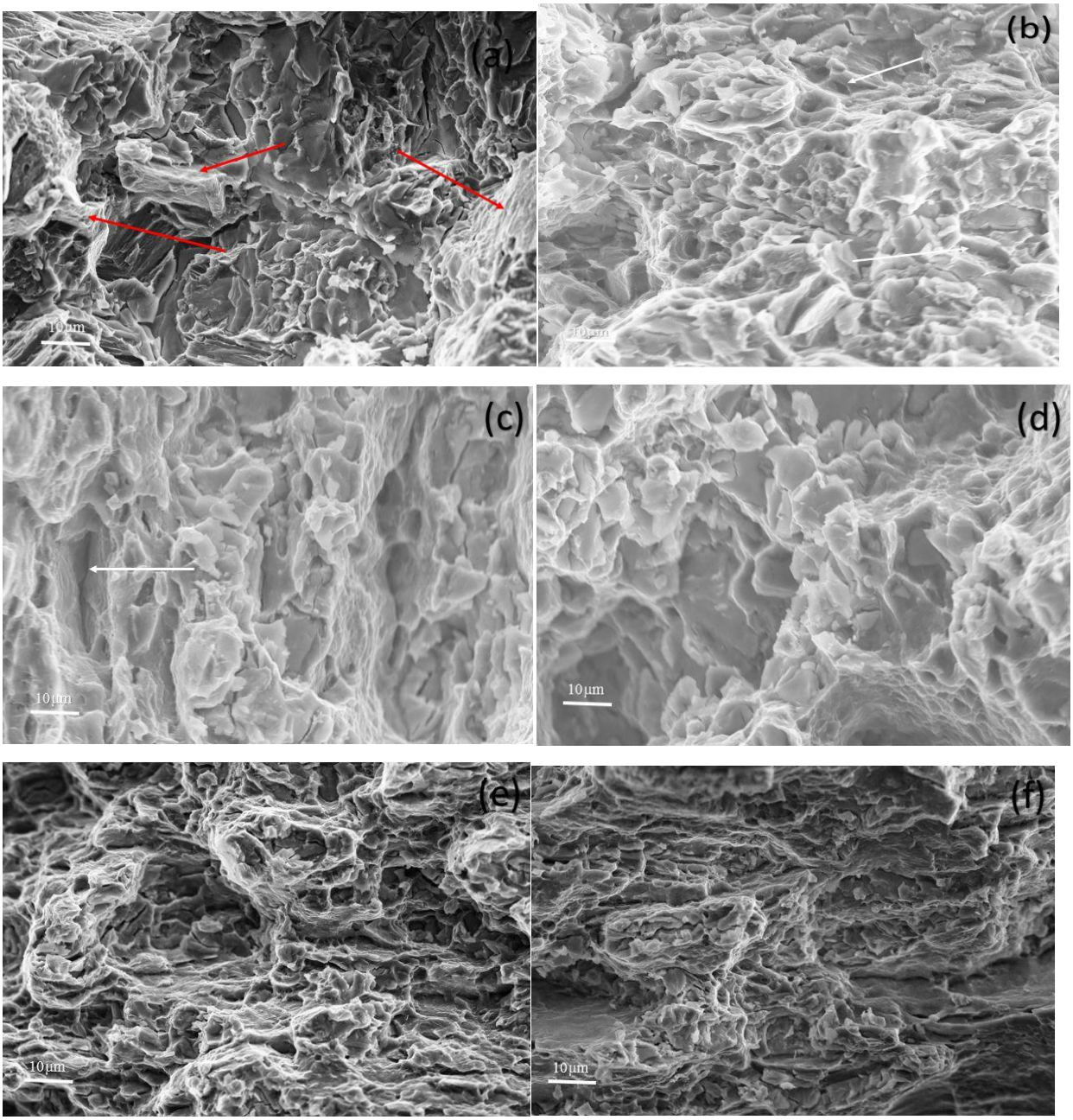

Fig. 6.8 Fractrography images of Tensile tested samples under (a) as Cast (b) 3 PF, (c) 3PF +70% Rolled, (d) 6PF, (e) 6 PF + 70% Rolled and (f) 70% rolled conditions.

6.2 Discussion

The results showed that the strength and ductility of the magnesium ZE41 alloy have been improved by MAF. The strengthening mechanisms in the ZE41 alloy includes dispersion strengthening, solid solution strengthening and grain refinement. Room temperature tensile ductility depends on the grain size of a commercially pure Mg, where a sharp ductility improvement was observed when the grain size decreased to less than 5μm. It was also found that the 80% of strain induced was accomplished by grain boundary sliding [12]. Therefore, the refinement of particle and grain size by MAF processing improves the ductility on the material. Ting et al. [10] reported that the structure containing ultrafine grains and weak texture can be successfully achieved using MAF after 6 passes in a magnesium rare earth alloy. The main mechanism of the grain refinement is dynamic recrystallization. The number of equi-axed grains increase with increasing the number of passes. Here in this work the increase in strength and ductility both is due to the dynamic recrystallization mechanism.

With increasing temperature, the main plastic deformation mechanism of the cast magnesium alloys change to dislocation slip from twinning at room and low temperature. In as casted sample twinning is observed but, as the other processing are done on high temperatures, so there is very less or no twinning occurs in the material. At room and low temperatures twinning mainly dominating deformation mechanism, and this restricts the ductility of HCP magnesium alloys with coarse grain structure due to limited number of slip systems available. This unusual increment in both strength and ductility of the alloy can be due to the presence of lower fraction dislocation density and higher high angle grain boundaries. Crystallographic glide and grain boundary sliding are the two well-known independent mechanisms for any metallic system, out of which one requiring lesser energy will be the favorable mode for the given experimental conditions. Equiaxed fine grains having high angle grain boundary undergoes grain boundary sliding more favorably.

As shown in Fig. 6.6 (b), the 3 pass sample consists of large grains, of about 60μm and very fine grains of about 1μm. The main mechanism of the grain refinement is dynamic recrystallization and this recrystallization starts at the grain boundaries. The fraction of large grains is more than the fine grains. This means that the main deformation mechanism is dependent on the large grains. Hence, crystallographic deformation is the principle deformation mechanism in as cast, T5 treated

and 3 pass forged samples. The large gains are not capable of accumulating dislocations. This is the reason for low ductility in these samples.

The 6-pass forged sample have ultrafine grained structure and equiaxed grains having large misorientation angles due to dynamic recrystallization, because of which the strength of the sample is higher than as cast sample. The ductility has not shown any significant improvement in the 3 and 6 pass sample, but the strength of the alloy is increased by 60%. This is because of the dislocation pile up in the grain boundaries which act as the barrier for the deformation and hence increases the strength. The ductility of the alloy has not sacrificed for this increment in strength.

The 3pass followed by 70% rolling sample show a very large increase in both ductility and strength. This can be attributed to the reduction in grain size on further rolling. The average grain size of the 3 pass sample has decreased further due to large strain rolling by the mechanism of dynamic recrystallization. Hence according to Hall-Petch relationship these fine grains may improve the strength of the material. In only rolled sample the improvement in strength can be attributed to several factors, mainly due to the refinement in grain size and also due to presence of the dislocations increasing at the grain boundaries. The rolled samples after 3 pass and 6 pass forging consists equiaxed ultrafine grains with large misorientation angles as a result of dynamic recrystallization due to which the elongation to failure is higher than the as casted samples. This high ductility means occurrence of grain boundary sliding in the ufg microstructure. In fine dynamically recrystallized grains the grain boundary sliding is accommodated by grain boundary diffusion and intergranular slip. Therefore, crystallographic glide (twinning/slip) and grain boundary sliding combined may be the possible mechanism for deformation in the fine grain structure. The mechanism of deformation was investigated using fractrography using SEM, as represented in Fig. 6.8. Therefore, the main reason for the excellent mechanical properties of the ultrafine grained ZE41 magnesium alloy are probably lower intergranular dislocation density and high amount of high angle grain boundaries. Increase in strain hardening may be due to the fact that the grain boundaries are more effective in blocking slipping dislocations, which in turn forces the dislocations to tangle and agglomerate near the grain boundaries. Grain boundary sliding will result in the emission of dislocations at triple junctions because of high stress concentration increasing strain-hardening rate.

6.3 Simulation Results

Finite element simulations were carried out using ANSYS 15.0 software. Non-linear static structural analysis was done for verifying the stress-strain experimental results and then fatigue and fracture simulations were carried out using the experimental stress-strain data. Mesh optimization showed that the optimum element size for tensile test specimen was 0.05mm and that for fatigue simulations it was 0.1mm.

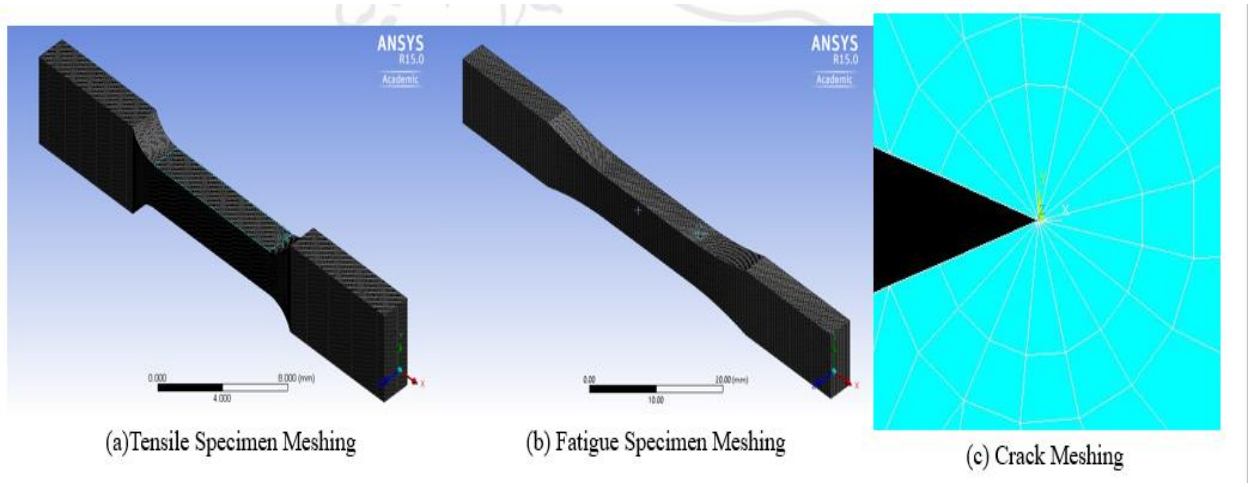

Fig. 6.9 Different meshing used for finite element simulations.

6.3.1 Tensile Test Simulations

The tensile test simulations were carried out using ANSYS Workbench 15.0. The specimen used for simulations was designed from ASTM standard B557 [55] having gauge length of 10mm shown in Fig. 6.9 (a).

The nonlinear static analysis was carried out for finding out the stress strain curve from the finite element analysis. The plastic strain data was introduces in the analysis from the experimental stress strain curve. The results obtained from the finite element simulations are comparable to the experimental results. The tensile test simulation stress strain curves are plotted for various conditions which are as shown in Fig. 6.10.

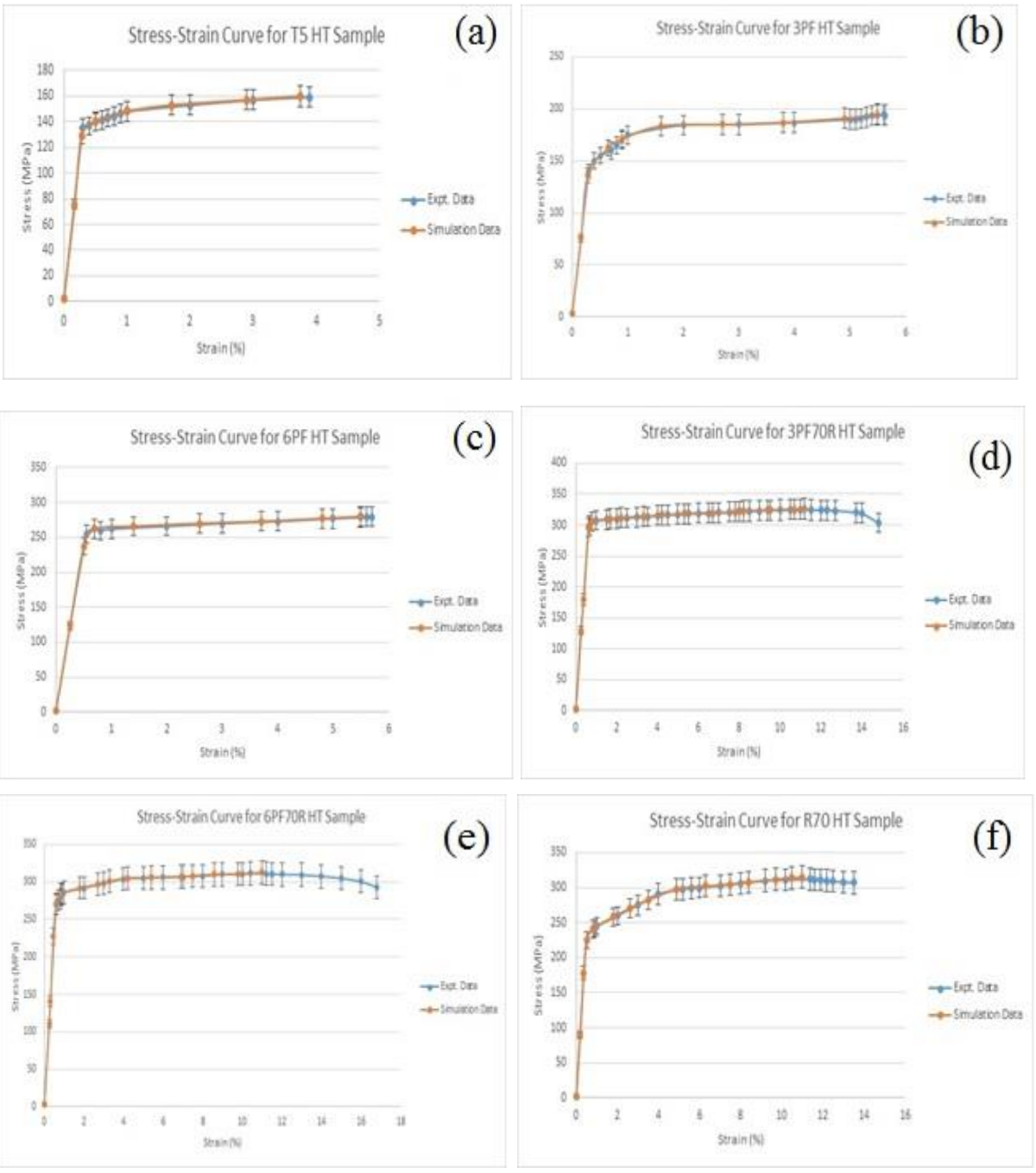

Fig. 6.10 Stress-Strain Curve obtained from Finite Element Analysis for different condition samples compared with the experimental results. (a) T5, (b) 3PFHT, (c) 3PF70RHT, (d) 6PFHT, (e) 6PF70RHT, (f) 70RHT.

6.3.2 Fracture Mechanics

Fracture mechanics simulations were carried out using ANSYS APDL and Workbench software. The stress strain data obtained from the experiments were used to perform the fracture simulations. Linear elastic fracture and elasto-plastic fracture mechanics approach was carried out for simulations. To compare the fracture properties of the as cast and processed magnesium ZE41 alloy J-integral was calculated for some 2-D cracked specimens having displacement controlled loading under plane stress and plane strain conditions. Different displacement applied for computing the J-integral of the fracture specimens with constant crack length. An effective improvement in the J-integral values was observed due to increase in strength of the processed specimens.

Case I- Edge-Crack Model under mode-I loading

The edge cracks are mainly developed on the surfaces on the component due to any impact or due to rough polishing. A 2-D specimen (60mm×50mm) having a crack length of 15mm on the edge was used for the analysis of the alloy with different processing conditions. ¼ skewed mesh with 6 counters around the crack tip was used with Plane 182 element for both plane stress and plane strain fracture mechanics analysis to compare the J-integral values of different condition processed alloy.

The J-Integral values for different condition processed alloy are plotted in Fig. 6.11 for both plane stress and plane strain conditions. From the graph it may be observed clearly that the J-Integral values increased with increasing the strength of the alloy. These plots suggests that with increase in strength of the alloy, the capability to arrest the crack is also increasing. The plastic region near the crack tip shows almost no change for as cast, 3-pass forged and 6 pass forged alloy, but it shows increment in plastic region around the crack tip for the rolled sample, followed by 3-pass forged + 70% rolled and 6-pass forged + 70% rolled alloy, for a displacement of 0.5mm, which showed the increased plasticity of the processed alloys due to rolling at high temperature and with increasing strain, as shown in Fig 6.12 for plane strain conditions.

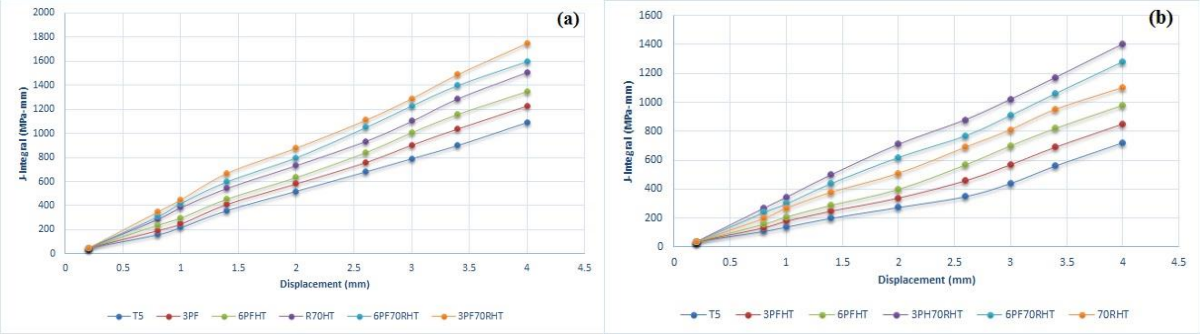

Fig. 6.11 Simulation results for an edge-crack specimen (a) J-Integral under plane strain, (b) J-Integral under plane stress.

Case II- Centre-Crack Model under mode-I loading

In any fracture mechanics analysis, the simulations of center crack in a specimen is common as these type of cracks are formed in material during the casting process. A 2-D specimen having dimensions (50mm×60mm) and crack length of 15mm at the center was taken to analyze different conditions processed alloy. ¼ skewed mesh with 6 counters near the crack tip with Plane 182 element was used for the calculation of J-Integral calculations.

The results of J-integral calculations are plotted in Fig. 6.13 for different conditions of processing on the alloy. From the graph it can be clearly observed that there is increase in J-Integral value with increasing the deforming strain. The plastic region formed near the crack tip are shown in Fig. 6.14 for different condition samples under plane strain analysis. The J-Integral values for center crack are lesser than the edge crack, which shows that lesser amount of energy is required to propagate a center crack in the specimen.

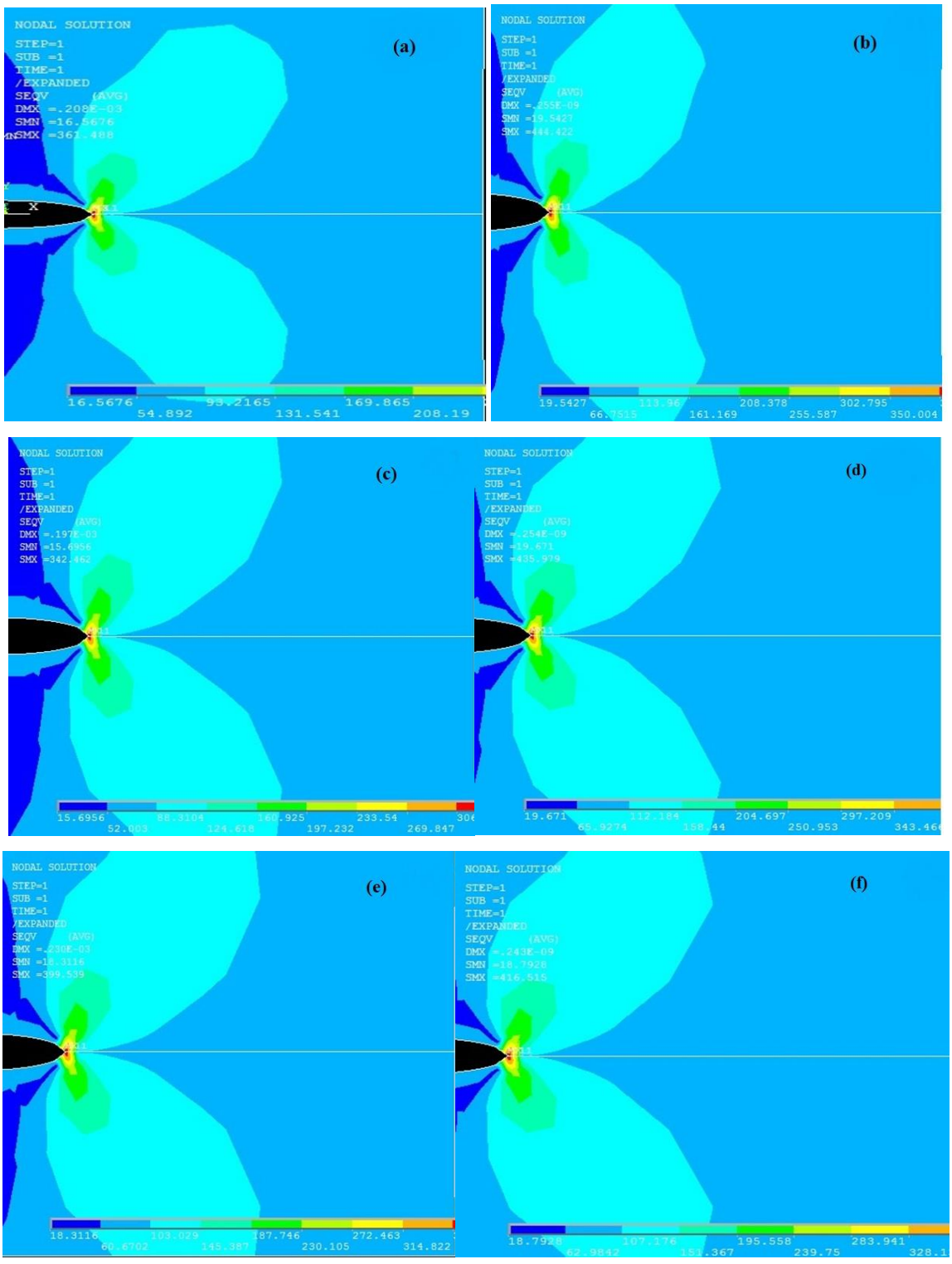

Fig. 6.12 Crack-tip Von-Mises stress for a single edge crack specimen corresponding to 0.5 mm displacement at different processing conditions under plane strain condition (a) 6PFHT, (b) 3PF70RHT, (c) 6PF70RHT, (d) 70RHT.

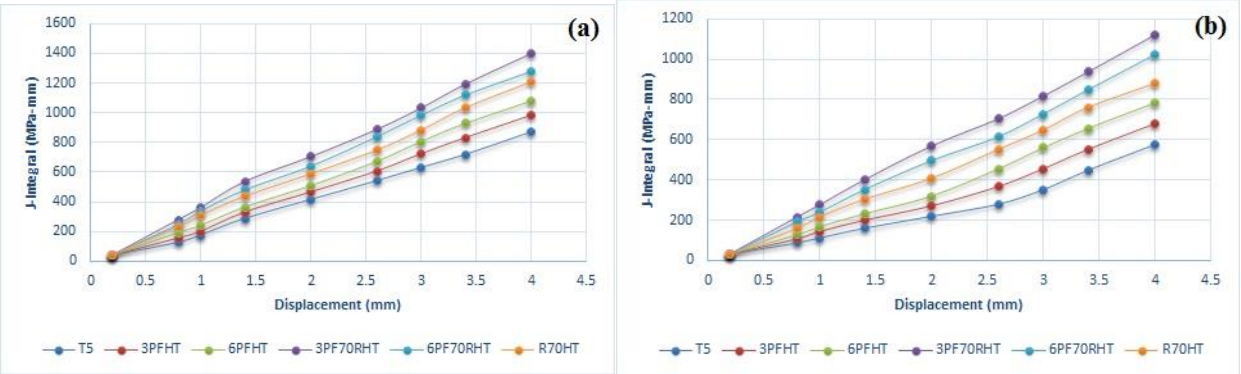

Fig. 6.13 Simulation results for a center crack specimen (a) J-Integral under plane strain, (b) J-Integral under plane strain.

Case III: Double Edge-Crack Model under mode-I loading

This type of crack is not commonly seen in practice as the casted alloys has a lot of defects which are reduced using different mechanical processing such as rolling, forging, extrusion and by post or pre annealing. A 2-D specimen with dimensions (50mm×60mm) having a crack length of 10mm on each side edge was used to analyze the J-Integral values for the alloy with different processing conditions. ¼ skewed mesh with 6 counters near the crack tip with Plane 182 element was used for the simulations.

The calculated J-Integral values from the simulations are plotted in Fig. 6.15 for both plane stress and plane strain conditions. There is clear increase in the J-Integral values with increasing the deformation strain on the alloy, which shows that the crack arresting capability has been increased through the SPD processing. With increase in ductility the plastic region near the crack tip increases, which shows that the crack need more stress to propagate.

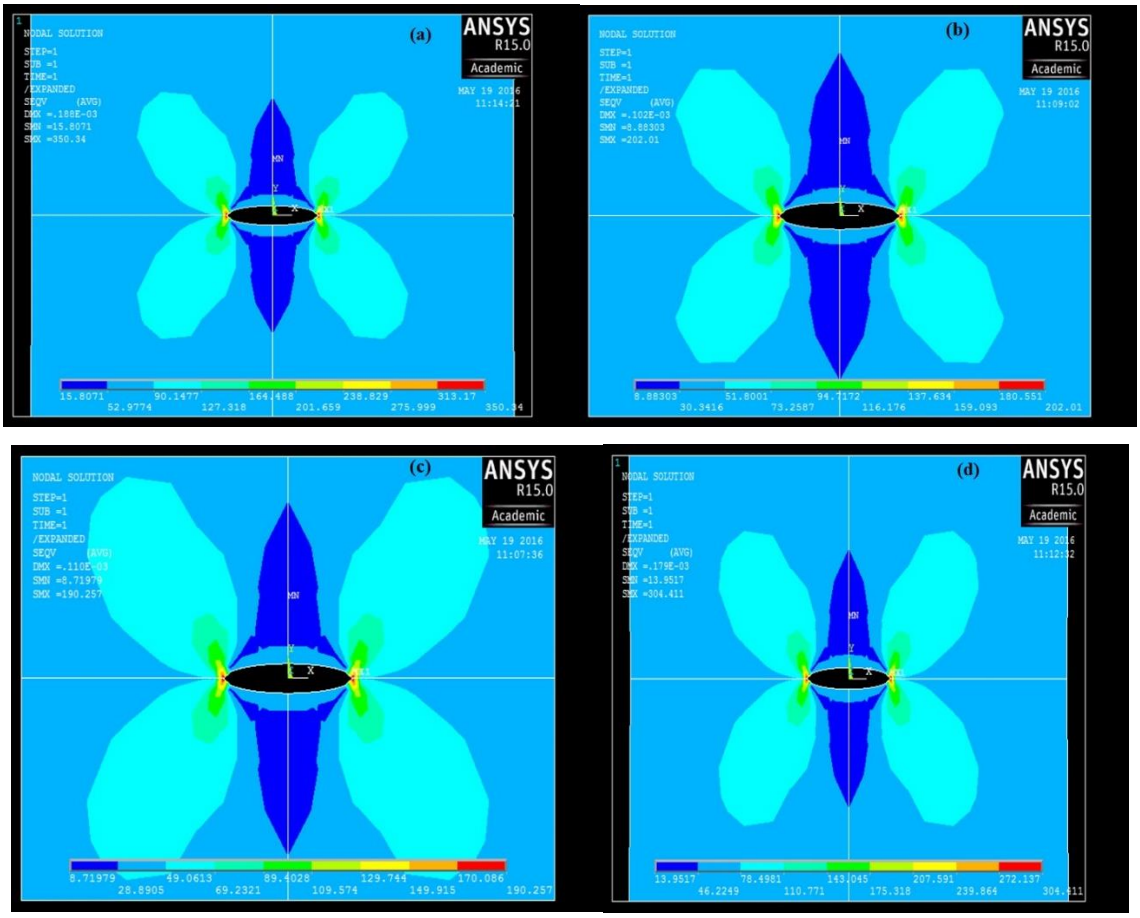

Fig. 6. 14 Crack-tip Von-Mises stress for a center crack specimen corresponding to 0.5 mm displacement at different processing conditions under plane strain condition (a) 6PFHT, (b) 3PF70RHT, (c) 6PF70RHT, (d) 70RHT.

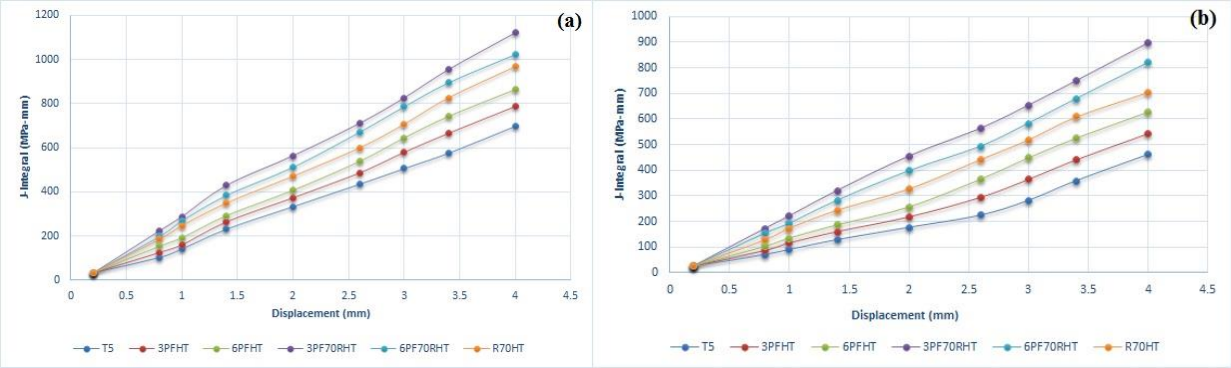

Fig. 6.15 Simulation results for a double edge crack specimen (a) J-Integral under plane strain, (b) J-Integral under plane strain.

6.3.3 Fatigue Simulations

Fatigue simulations for the different condition processed alloy were performed using ANSYS Workbench Software. Gerber's criterion for evaluating the fatigue life of the material is assumed to be more accurate for ductile materials as it treats both positive and negative stresses while others do not include both. Gerber's criterion for fatigue life can be represented as:

$$\frac{\sigma_{alternating}}{\sigma_{endurance\ limit}} + \left(\frac{\sigma_{mean}}{\sigma_{ultimate\ strength}}\right)^2 = 1$$

First of all, the results for the as castes alloy were compared with the results present in the literature [55]. These results showed that S-N curve obtained from the simulations were in good agreement with the results present in the literature. The results of the as casted alloy were compared with the other condition processed alloy, as shown in Fig. 6.16 (a). The S-N curve obtained from the simulations is represented in Fig. 6.16 (b). It can be sheen that the maximum number of cycles to failure for a given stress amplitude was shown by the 6-pass forged followed by 70% rolled sample. This is due to increase in both yield strength and ductility because of the processing at high temperatures. Many defects may develop due to the generation of dislocations inside the crystals with the application of cyclic loading, and start accumulating and propagating. This can also be stated that the fatigue life is more for more ductile sample. This can also be seen from the results obtained here from the simulations.

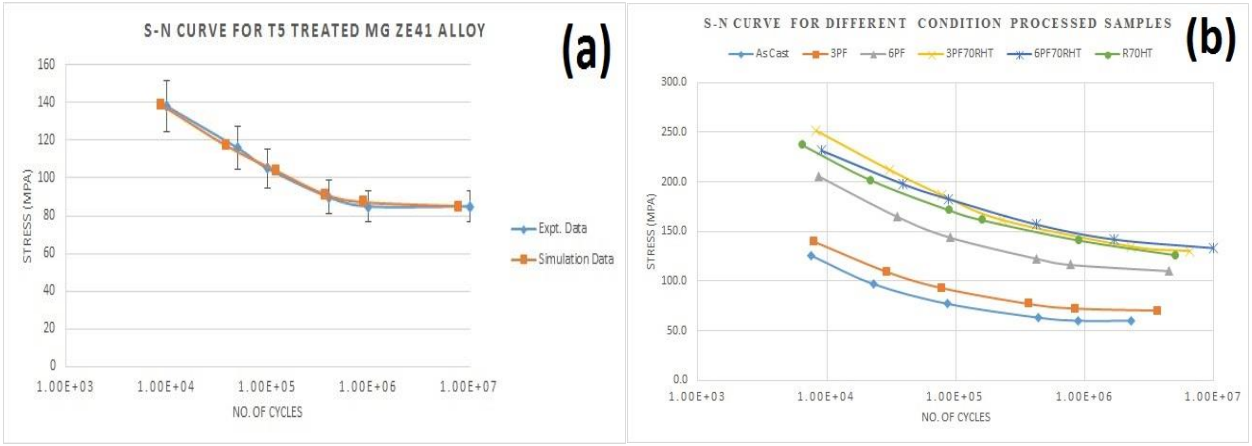

Fig. 6.16 (a) Comparison of fatigue results obtained from simulation with that of experimental results available in literature, (b) comparison of simulation results of fatigue life of different condition processed samples.

Conclusion

The casted alloy of magnesium ZE41 was processed through SPD route to produce ultrafine grained microstructure. The alloy was processed without heat treatment and also with T5 heat treatment. The alloy was forged and rolled at high temperature for producing the ultrafine grained microstructure. Fatigue and fracture properties of the processed alloy were studied and compared with the unprocessed alloy. The experimental results of the tensile, fatigue and fracture properties were also verified using finite element simulations. Following conclusions can be drawn from the present work:

- The properties of the Non heat treated alloy processed through different routes showed a sudden increment just after 3-pass forging but after that the properties get degraded.
- The tensile strength of the alloy after 3-pass forging at 450ºC followed by 70% rolling at 450ºC increased to 325 MPa from the initial of 160 MPa.
- The elongation to fracture of the alloy after 6-pass forging at 450ºC followed by 70% rolling at 450ºC increased from 4% to 16.8%.
- The alloy showed a unique combination of increase in both strength and ductility.
- The alloy exhibited an ultrafine grained microstructure with grain size of about 1µm for the alloy processed with 3-pass forging followed by 70% rolling and grain size of 700nm for the alloy processed with 6-pass of forging.
- The fracture toughness of the alloy increased by about 60% by processing through 6-pass forging followed by 70% rolling.
- Fatigue life of the processed alloy was found out using finite element simulations showed a clear improvement in the life of the specimen with increasing the deformation strain.
- The fracture mechanics simulations showed that the crack arresting capability of the alloy was increased for the processed alloy at higher deformation strain.

Suggestion for Future Work

In the present study the mechanical behavior of the magnesium ZE41 alloy was thoroughly studied by conducting experiments and simulations. The alloy finds its applications mostly in the aviation industry. The main problem with this alloy is also its high corrosion rate. So, following studies can be conducted for this alloy:

- The tensile strength at elevated temperatures and also at subzero temperatures.
- The fatigue testing of the processed alloy experimentally.
- Corrosion testing of the processed alloy to see if the corrosion properties has also been increased by the processing.

References

1. B.L. Mordike and T. Ebert, "Magnesium: Properties- applications- potential", *Materials Science and Engineering A* 302 (2001) pp. 37-45.
2. M. Avedesian and H. Baker, "ASM Specialty Handbook: Magnesium and Magnesium Alloys", *ASM International*, (2009), pp.3-6.
3. M.B. Kannan and R.K.S. Raman, "Magnesium Alloys as Biodegradable Implants", *Materials Science Forum,* 618-619 (2009), pp. 83-86.
4. W. Zhaoxuan and W.A. Curtin, "The origin of High Hardening and Low ductility in Magnesium" *Nature Article,* 526, (2015), pp. 62-67, doi: 10.1038/nature15364.
5. F.A. Mirza and D.L. Chen, "Fatigue of rare-earth containing magnesium alloys : a review," *Fatigue & Fracture of Engineering Materials and Structures,* vol. 37, January (2014), pp. 831–853.
6. C. Koch, "Chapter 6: Bulk Behavior of Nanostructured Materials," *Nanostructured Materials,* (1983), pp. 93–112.
7. O. Sitdikov and R. Kaibyshev, "Dynamic Recrystallization in Pure Magnesium", *Materials Transactions,* 42, no. 9 (2001), pp. 1928-1937.
8. S.E. Ion, F.J. Humphreys and S. H. White, "Dynamic Recrystallization and the Development of Microstructure during the High Temperature Deformation of Magnesium", *Acta Metallurgica,* 30 (1982), pp. 1909-1919.
9. T. Al-Samman and G. Gottstein, "Dynamic Recrystallization during High Temperature Deformation of Magnesium", *Materials Science and Engineering A,* 490 (2008), pp. 411-420.
10. L. Ting, Z. Kui, D. Zhiwei, Y. Jiawei and L. Xinggang, "Production of fine-grained and weak texture structure in an Mg-7Gd-5Y-1Nd-0.5Zr alloy by multi-axial forging", *Applied Mechanics and Materials*, vols. 633-634 (2014), pp. 120-124.
11. R.B. Figueiredo, T.G. Langdon, "Principles of grain refinement and superplastic flow in magnesium alloys processed by ECAP", *Materials Science and Engineering A,* 501 (2009), pp. 105–114.
12. R. Ding, C. Chung, Y. Chiu and P. Lyon, "Effect of ECAP on microstructure and mechanical properties of ZE41 magnesium alloy", *Materials Science and Engineering A,* 527 (2010), pp. 3777–3784.

13. M. Aibin, J. Jiang, N. Saito, I. Shigematsu, Y. Yuan, D. Yang and Y. Nishid, “Improving both strength and ductility of a Mg alloy through a large number of ECAP passes”, *Materials Science and Engineering A*, 513–514 (2009), pp. 122–127.
14. L. Ting, Z. Kui, L. Xinggang, D. Zhiwei, L. Yongjun, M. Minglong and S. Guoliang, “Dynamic precipitation during multi-axial forging of an Mg-7Gd-5Y-1Nd-0.5Zr alloy”, *Journal of Magnesium and Alloys,* 1 (2013), pp. 47-53.
15. H. Gleiter, “Nanocyrstalline Materials”, *Progress in Materials Science,* vol. 33, (1989), pp. 223–315.
16. A. Galiyev, R. Kaibyshev, G. Gottstein, “Correlation of plastic deformation and dynamic recrystallization in magnesium alloy ZK60”, *Acta Metallurgica*, 49 (2001), pp. 1199–1207.
17. H. Q. Sun, Y. N. Shi, M. X. Zhang and K. Lu, “Plastic strain- induced grain refinement in nanometer scale in a Mg Alloy”, *Acta Materialia,* 55 (2007), pp. 975-982.
18. M.M. Pour, M.H. Parsa, A. Khajezade and H. Mirzadeh, “Multi-Axial Incremental Forging and Shearing as a New Severe Plastic Deformation Processing Technique”, *Advanced Engineering Materials,* 17, no. 8 (2015), pp. 1197-1207.
19. B. Gwynne and P. Lyon, “Magnesium Alloys in Aerospace Applications, Past Concerns, Current Solutions”, *Triennial International Aircraft Fire & Cabin Safety Research Conference,* October 29 - November 1, (2007).
20. D. Aurbach, Z. Lu, A. Schechter, Y. Gofer, H. Gizbar, R. Turgeman, Y. Cohen, M. Moshkovich and E. Levi, “Prototype systems for rechargeable magnesium batteries”, *Nature*, Vol 407 (2000), pp. 724-727.
21. O. Chusid, Y. Gofer, H. Gizbar, Y. Vestfrid, E. Levi, D. Aurbach, and I. Riech, “Solid-State Rechargeable Magnesium Batteries”, *Advanced Materials,* 15, no. 7-8 (2003), pp. 627-630.
22. M.T. Perez-Prado, J. A. del Valle and O.A. Ruano, “Grain refinement of Mg–Al–Zn alloys via accumulative roll bonding”, *Scripta Materialia*, 51 (2004), pp. 1093–1097.
23. M. Kai, Z. Horita, and T.G. Langdon, “Developing grain refinement and superplasticity in a magnesium alloy processed by high-pressure torsion”, *Materials Science and Engineering A*, 488 (2008), pp. 117–124.

24. Q. Chen, D. Shu, C. Hu, Z. Zhao, and B. Yuan, “Grain refinement in an as-cast AZ61 magnesium alloy processed by multi-axial forging under the multi-temperature processing procedure”, *Material Science and Engineering A*, vol. 541 (2012), pp. 98–104.
25. S.K. Panigrahi and R. Jayaganthan, “Development of ultrafine grained high strength age hardenable Al 7075 alloy by cryorolling”, *Materials and Design*, 32 (2011), pp. 3150–3160.
26. O. Zienkiewicz and R. Taylor, “The finite element method for solid and structural mechanics”, *Elsevier*, (2005).
27. M. Aliabadi, “The boundary element method”, Volume 2, Applications in solids and structures. *Wiley* (2002).
28. M. Bonnet, “Boundary integral equation methods for elastic and plastic problems”, *Encyclopedia of Computational Mechanics*, vol. 2 (2004).
29. J. Melenk and I. Babuka, “The partition of unity finite element method: basic theory and applications”, *Computer methods in applied mechanics and engineering*, vol. 139, no. 1-4 (1996), pp. 289–314.
30. T. Strouboulis, K. Copps and I. Babuska, “The generalized finite element method”, *Computer Methods in Applied Mechanics and Engineering*, vol. 190, no 32-33 (2001), pp. 4081–4193.
31. N. Moes, J. Dolbow and T. Belytschko, “A finite element method for crack growth without remeshing”, *International Journal for Numerical Methods in Engineering*, vol. 46, no. 1 (1999), pp. 131–150.
32. A. Griffith, “The Phenomena of Rupture and Flow in Solids”, *Philosophical Transactions of the Royal Society of London, Series A*, vol. 221 (1921), pp. 163–198.
33. J. Rice, “A path independent integral and the approximate analysis of strain concentration by notches and cracks”, *Journal of Applied Mechanics*, vol. 35, no. 2 (1968), pp. 379–386.
34. J. Eshelby, “The continuum theory of lattice defects”, *Solid State Physics*, vol. 3 (1956), pp. 79–144.
35. T. Anderson, “Fracture mechanics: fundamentals and applications”, *CRC*, (2005).
36. C. Desrayaud, S. Ringeval, S. Girard, and J. H. Driver, “A novel high straining process for bulk materials - The development of a multipass forging system by compression along

three axes", *Journal of Materials Processing Technology*, vol. 172, no. 1 (2006), pp. 152–158.

37. S. Goel, G. Kumar, R. Jayaganthan, I.V. Singh, D. Srivastava, G.K. Dey and N. Saibaba, "Experimental evaluation of mechanical properties and fracture-fatigue simulation of cryo and room temperature rolled zircaloy–2", *International Journal of Microstructure and Materials Properties,* vol.9, no. 2 (2014), pp. 120-135.
38. http://www.magnesium-elektron.com/sites/default/files/Elektron%20RZ5_0.pdf, date-21/03/2016, 1.00AM.
39. A. Azushima, R. Kopp, A. Korhonen, D.Y. Yang, F. Micari, G.D. Lahoti, P. Groche, J. Yanagimoto, N. Tsuji, A. Rosochowski and A. Yanagida, "Severe Plastic Deformation (SPD) for Metals", *CIRP Annals – Manufacturing Technology*, 57 (2008), pp. 716-735.
40. T.G Nieh and J. Wadsworth, "Hall Patch Relation in Nanocrystalline Solids", *Scripta Metallurgica,* 25 (1991), pp. 955-958.
41. H. Somekawa, A. Singh and T. Mukai, "High fracture toughness of extruded Mg–Zn–Y alloy by the synergistic effect of grain refinement and dispersion of quasicrystalline phase", *Scripta Materialia,* 56 (2007), pp. 1091–1094.
42. H. Somekawa and T. Mukai, "Fracture toughness in Mg–Al–Zn alloy processed by equal-channel-angular extrusion", *Scripta Materialia,* 54 (2006), pp. 633–638.
43. T. Inoue, Y. Kimuraa and S. Ochiaib, "Static fracture toughness of fail-safe steel", *Scripta Materialia,* 65 (2011), pp. 552–555.
44. P. Kumar, "Elements of Fracture Mechanics", *McGraw-Hill Education Private Limited*, India (2013), pp. 155-171.
45. T. Shimokawa, M. Tanaka, K. Kinoshita and K. Higashida, "Roles of Grain Boundaries in improving fracture toughness of ultrafine-grained metals", *Physics Review B*, 83 (2011).
46. W.M. Garrison Jr and N.R. Moody, "Ductile Fracture", *Journal of Physics and Chemistry of Solids*, 48 (1987), pp. 1035-1074.
47. M.A. Meyers, A. Mishra and D.J Benson, "Mechanical Properties of Nanocrystalline Materials*", Progress in Material Science,* 51 (2006), pp. 427-556.
48. L. Zhu and Z. Lu, "Modelling the plastic deformation of nanostructured metal with bimodal grain size distribution", *International Journal of Plasticity*, 30-31 (2012), pp. 166-184.

49. P. Das., R. Jayaganthan and I.V. Singh, "Tensile and Impact Toughness Behaviour of Cryorolled Al 7075 alloy", *Materials & Design*, 32 (2011), pp. 1298-1305.
50. ANSYS Element Reference, (2009), pp. 1189-1204 and 1327-1358.
51. ANSYS Mechanical APDL Structural Analysis Guide, (2015), pp. 339-379 and 423-433.
52. J.W. Hutchinson, "Singular Behavior at the End of a Tensile Crack in a Hardening Material." *Journal of the Mechanics and Physics of Solids*, 16, 1 (1968), pp. 13-31.
53. J.R. Rice and G. F. Rosengren. "Plane Strain Deformation near a Crack Tip in a Power Law Hardening Material." *Journal of the Mechanics and Physics of Solids*, 16 (1968), pp. 1-12.
54. ANSYS Mechanical APDL Theory Reference, (2015), pp. 5-28 and 859-861.
55. J.J. Bethke, "Effect of corrosion Resistant coatings of the Fatigue Strength of Cast Magnesium Alloys" *Report No. NADC-77140-30* (1977), pp. 29-50.
56. ASTM Standard E399-12, "Standard Method for Linear Elastic Plane Strain Fracture Toughness K_{IC} of Metallic Materials", (2013), pp. 1-33.
57. ASTM Standard E1820-15a, "Standard Method for Measurement of Fracture Toughness", (2015), pp. 1-53.
58. ASTM Standard E466-15, "Standard Practice for Conducting Force Controlled Constant Amplitude Axial Fatigue Tests of Metallic Materials", (2013), pp. 1-6.
59. X.K. Zhu and J.A. Joyce, "Review of fracture toughness (G, K, J, CTOD, CTOA) testing and standardization", *Engineering Fracture Mechanics*, 85 (2012), pp. 1–46